MICROSTRUCTURAL EVOLUTION AND THERMAL STABILITY OF AL-CE-NI TERNARY EUTECTIC

By

ERIC J. FODRAN

A DISSERTATION PRESENTED TO THE GRADUATE SCHOOL
OF THE UNIVERSITY OF FLORIDA IN PARTIAL FULFILLMENT
OF THE REQUIREMENTS FOR THE DEGREE OF
DOCTOR OF PHILOSOPHY

UNIVERSITY OF FLORIDA

2002

TABLE OF CONTENTS

page

ABSTRACT iv

CHAPTER

1 INTRODUCTION 1

2 LITERATURE REVIEW 5

Drivers and Requirements for Lightweight Materials for Elevated-Temperature Applications 5
Conventional Strengthening Mechanisms for Aluminum Alloy Systems 6
Oxide Dispersion Strengthened Systems 8
Rapidly Solidified Alloy Systems 9
History of Rapid Solidification of Aluminum Alloys 10
Powder metallurgy 10
Spray forming 11
Properties 11
Ternary Eutectic Systems 12
Bi-Cd-Sn System 13
Al-Cu-Ni and Cd-In-Sn Systems 14
Al-Ce-Ni Systems 15
Al-Ni and Al-Ce Binary Eutectic Systems 16

3 SOLIDIFICATION MICROSTRUCTURE SELECTION OF THE ALUMINUM-CERIUM-NICKEL TERNARY EUTECTIC SYSTEM 29

Background 29
Experimental Work 31
Results and Discussion 32
Conclusions 37

4 ELEVATED TEMPERATURE STABILITY OF ALUMINUM-CERIUM-NICKEL TERNARY EUTECTIC STRUCTURES 58

Background 58
Experimental Work 59

Results and Discussion 60
Conclusions 62

5 MICROSTRUCTURES AND CRYSTALLOGRAPHY OF THE DIRECTIONALLY SOLIDIFIED ALUMINUM-CERIUM-NICKEL TERNARY EUTECTIC SYSTEM 73

Background 73
Experimental Work 75
Results 77
Discussion 78
Conclusions 83

6 CONCLUSIONS 101

APPENDIX

A.. SELECTED AREA DIFFRACTION PATTERNS 103
B . VOLUME FRACTIONS OF PHASES IN TERNARY EUTECTIC 105
C . SURFACE AREA PER VOLUME FOR MINOR PHASES 106

BIBLIOGRAPHY 109

BIOGRAPHICAL SKETCH 119

Abstract of Dissertation Presented to the Graduate School
of the University of Florida in Partial Fulfillment of the
Requirements for the Degree of Doctor of Philosophy

MICROSTRUCTURAL EVOLUTION AND THERMAL STABILITY OF AL-CE-NI TERNARY EUTECTIC

By

Eric J. Fodran

August 2002

Chairman: Michael J. Kaufman
Major Department: Materials Science And Engineering

The engineering community has identified several applications in which the use of a lightweight alloy for elevated temperature service, in substitution for current heavier and more costly alloys, would have a substantial benefit. This need for structural materials to perform at elevated temperatures has driven researchers to develop novel alloys as well as processing routes to manufacture them and obtain optimum microstructures. Previous studies on aluminum based binary eutectic systems have proven that the aluminum alloy system shows promising potential for satisfying this need. This has motivated the investigation of the solidification and thermal stability of the Al-12 wt% Ce-5 wt% Ni ternary eutectic performed in this investigation. The solidification behavior of the Al-Ce-Ni ternary eutectic was conducted via solidification of various compositions at and above the eutectic composition in a copper chill mold, thus allowing the observation of various solidification rates on a single ingot. Directional

solidification of the ternary eutectic was also conducted to further study the unique microstructures forms. After casting the ingots were analyzed for the composition of phases in the microstructure via X-ray diffraction, and the distribution of the phases determined by scanning electron microscopy. The solidification of the ternary eutectic was found to occur much like that of a faceted/non-faceted binary couples growth. The thermal stability of the microstructure was also studied. Ternary eutectic microstructures were heat treated at various temperatures for time intervals up to 100 hours. The coupled growth microstructures were found to coarsen at temperature above 400°C, which was associated with a loss in hardness. Coarsening of the microstructures at elevated temperatures was also observed to occur by multiple mechanisms: an Ostwald ripening within the eutectic cell, and an accelerated coarsening at the cell boundaries due to increased diffusion at boundaries. Unique ternary eutectic structures were found to be comprised of a fine distribution of chains of alternating Al11Ce3 and Al3Ni intermetallics in an aluminum matrix. The unique microstructures formed are believed to be driven by the solute diffusion profile at the solid/liquid interface during solidification. This suggests that it may not be possible to generate a microstructure comprised of a homogeneous distribution of multiple product phases in a continuous matrix on solidification from a single parent phase, such as that of the solidification of ternary eutectics.

CHAPTER 1
INTRODUCTION

Aluminum-based alloys have been investigated for several years as alloy systems with expansive potential within the aircraft and automotive industries. This is largely due to their low density, high specific strength, low cost, and reasonable corrosion resistance in most environments due to the adherent Al_2O_3 passivating film.[2,3] As a result of research and development, aluminum-based alloys are extensively used in applications which require a low-density material to exhibit strength performance at near-ambient temperatures. In the case of conventional large and small airframes, for example, up to 70-80% of their structural weight is comprised of aluminum-based alloys.[4]

The majority of the conventional aluminum alloys in application are strengthened via precipitation hardening.[4] While these alloys exhibit favorable strengths (σ_{YS} = 475 MPa for 7075-T6) and are low in density (2.8 g/cm^3 for 7075), they are not suitable for applications at slightly elevated temperatures, since the strengthening phases coarsen and/or dissolve into solution.[5] The temperature at which this microstructural instability occurs varies depending on the specific alloy, but commonly occurs at or above 100°C for current precipitation hardened alloys.[5] The artificially aged 7075 alloy in the T6 condition, for example, retains only 43% of its room temperature tensile strength (525 MPa) at 150°C after exposure for 1000 hours.[5]

Alternatives to the precipitation strengthened alloy systems include the commercial Al-Si cast alloys which maintain their mechanical properties to intermediate temperatures.[5] The Al-Si based 336 alloy, for example, exhibits a room temperature tensile strength of 248 MPa and retains 85% of its room temperature strength at 150°C after exposure for 1000 hours.[5] Although this and other cast alloys (i.e., alloys 339 and 390) retain their mechanical properties at elevated temperatures far better than the wrought precipitation hardened alloys, their maximum strengths are considerably lower (~285 MPa).[5]

To further address the need to develop light-weight structural materials for elevated temperature applications, oxide dispersion strengthened (ODS) alloys were investigated.[6-8] The dispersion of a fine distribution of stable oxides in aluminum matrices results in an increased thermal stability of the microstructure. ODS alloys were shown to retain their mechanical properties much better in comparison to precipitation hardened alloys, retaining 83% of their room temperature yield strength at 150°C and 61% at 300°C. However, as in the case of the Al-Si cast alloys, the maximum strength of the ODS alloys was considerably lower in comparison with the wrought precipitation hardened aluminum alloys.[6] Rapid Solidification Processing (RSP) techniques have also been employed in attempts to obtain high strength aluminum alloys which exhibit microstructural stability at elevated temperatures. Such techniques, while economically costly, were successful in obtaining fine dispersions of intermetallic particles in the aluminum matrix, resulting in desirable tensile strengths of up to 580 MPa.[7-9] In most cases, however, the resultant microstructures proved to be

unstable, either coarsening or transforming to other phases at elevated temperatures.[8-10] The inability of such techniques to produce an aluminum alloy which exhibits high strength and microstructural stability at elevated temperatures thus motivates further investigation into alternative aluminum alloy systems and/or processing techniques. In the hopes of obtaining microstructures comprised of a fine distribution of strengthening phases from the melt, the casting of ternary eutectic alloys has been identified as a potential alternative and more economic approach for obtaining strong aluminum-based alloys which exhibit microstructural stability at elevated temperatures.[11,12]

Casting of eutectic compositions allows a low cost process for the solidification of potentially stable microstructures from the melt, which may resist further transformation upon service at elevated temperatures. Specifically, among the aluminum-based eutectic systems, a ternary eutectic comprised of a significant volume fraction of intermetallics in an aluminum matrix may be promising. An aluminum-rich ternary eutectic which solidified with a significant volume fraction of the intermetallic phases from the melt may prove to be applicable where moderate strength and strength retention at elevated temperatures are required. The Al-Ce-Ni system has been recognized as one such ternary eutectic which may be feasible.[1] Both the binary Al-Ce and Al-Ni systems have eutectic reactions at aluminum-rich compositions which result in significant volume fractions of intermetallics (i.e., 15% and 8% for the Al-Ce and Al-Ni systems, respectively).[13,14] In addition, no ternary Al-Ce-Ni phases are present in the aluminum-rich corner of this system.

To further complement the thermal stability and strength properties initially driving the study of the Al-Ce-Ni system, from the standpoint of further understanding of ternary eutectic reactions, the effects of such process variables as composition and cooling rate on microstructural evolution and microstructural optimization, the Al-Ce-Ni was believed to be a favorable choice for this study. Systematic control of composition and process variables to obtain a variety of compositions cast at varying solidification rates have been followed with comparisons on the following aspects: a) effect of eutectic and near-eutectic compositions on the ternary microstructure, b) correlation between resultant microstructures and mechanical properties, c) thermal stability of the microstructures, d) effect of directional solidification on microstructures and mechanical properties, and e) crystallography of the microstructures formed.

In addition to the need for lightweight high strength alloys,[4,15,16] there is a general lack of knowledge concerning the casting of ternary eutectic systems for structural applications at elevated temperatures. The insight gained from this study regarding the microstructural evolution and optimization of the Al-Ce-Ni ternary eutectic is also focused towards a greater understanding of ternary eutectic systems and their resulting microstructures.

CHAPTER 2
LITERATURE REVIEW

Drivers and Requirements for Lightweight Materials for Elevated-Temperature Applications

The search for lightweight alloys capable of maintaining strength at elevated temperatures has been actively pursued in both the aerospace and automotive communities.[4,15,16] Several of the material requirements which must be met include formability, machinability, low density, environmental resistance, strength retention at elevated temperatures, and cost, which must be justified by material performance.

Aluminum-based alloy systems are currently some of the most widely employed structural materials in the commercial aircraft industry.[4] They derive their success as a structural material from a unique combination of strength, low density, versatility, and economy.[3,4,17] Significant advances in aluminum alloy technology have allowed for greater efficiency, decreased fuel consumption, and greater payload capabilities.[4] However, advances in the conventional aluminum systems to date have yet to achieve a lightweight material which can maintain its performance at elevated temperatures.

There are several areas for the application of a thermally stable, lightweight alloy system that have been identified in transportation and missile systems.[8,18,19] For example, a wide range of missiles travel within supersonic

velocities. Such velocities result in significant structural heating.[19,20] Use of aluminum alloys for these missile applications would require short exposure times of up to 160 s at Mach 3 to 4 velocities for some missiles, corresponding to 475 to 700°K (202 - 427°C) exposures.[19-21] Traditionally, more thermally stable titanium structural materials have been selected over aluminum for such applications, but impose significant weight increases which can decrease performance or prove to be unacceptable.[18] Similar arguments have also been made for the need for alloys with increased performance in the low-temperature fan and compressor sections of gas turbine engines.[16] Therefore, engineers continue to search for new aluminum alloy systems with improved high temperature performance.

There are several requirements which structural materials must meet for both the high velocity missile and gas turbine engine applications, the most critical of them being low density and high strength.[4,8,22] Accompanying the enhancement in performance due to the application of low density materials, the weight savings also result in a substantial reduction in operating cost.[8,23,24] Aluminum has a reasonably low density (2.69 g/cm^3)[2] and, although the strength of commercially pure aluminum is quite low (~75 MPa), current commercially available alloys have strengths that readily exceed 500 MPa.[3]

Conventional Strengthening Mechanisms of Aluminum Alloy Systems

Several strengthening methods are currently employed in conventional aluminum alloy systems. These include work hardening, solid solution hardening, solidification of hard reinforcing phases from the melt, and precipitation

hardening.[5,25,26] Precipitation hardened alloys comprise a large portion of those used in commercial applications of both cast and wrought products. All of these strengthening mechanisms, however, involve the hindrance of dislocation motion through the aluminum matrix. For example, in the case of precipitation hardened alloys, after precipitation of a fine intermetallic phase within the aluminum matrix, the coherent or semi-coherent precipitates induce a strain field in the matrix, thus impeding dislocation motion and increasing strength.[26] Though precipitation hardened aluminum alloys exhibit high yield strengths of up to 475 MPa, their properties quickly deteriorate at elevated temperatures where the reinforcing precipitates either coarsen or dissolve into solution (Figure 2.1).

In the case of many aluminum casting alloys, in addition to precipitation hardening, strength is also attributed to the distribution of hard eutectic phases.[5] Additional alloying elements can also be added to refine the cast microstructure and further increase strength.[25] The Al-Si system is the basis for some of the most frequently utilized cast aluminum alloys. Several of these alloys (i.e., A336 and A390) exhibit superior microstructural stability at elevated temperatures and are commonly employed in automotive engine applications but have lower strength in comparison to the wrought precipitation hardened alloys.[5] A390, for example, exhibits a room temperature yield strength of 365 MPa and retains ~70% of its room temperature yield strength at 200°C. Overall, in comparison to the wrought precipitation hardened alloys, the cast alloys are superior in retaining their mechanical properties at elevated temperatures, but have a substantially lower strength.[5]

Oxide Dispersion Strengthened (ODS) Systems

Some of the early investigations in the development of Al-based alloys for elevated temperature service were conducted in the areas of oxide dispersion strengthening. The initial studies were performed via sintering aluminum powders with small volume fractions of Al_2O_3 in nitrogen atmospheres.[6] These processes resulted in microstructures consisting of an aluminum matrix with a dispersion of Al_2O_3 particles.[6] Within the aluminum matrix, the Al_2O_3 dispersion acts as non-shearable particles, which hinder the motion of dislocations.[6,27,28] It was found that ODS alloys exhibited an increased hardness as compared to sintered aluminum powders alone, and exhibited a yield strength which approached 200 MPa.[6] Additionally, due to the high temperature stability of the Al_2O_3 dispersion, ODS alloys retained their strength better at temperatures above 200°C in comparison to precipitation hardened alloys, retaining 83% of its room temperature yield strength at 150°C (Figure 2.2).[6] However, in addition to the high costs of the processing associated with the ODS alloys, due to the lower volume fraction of dispersoids and their larger size, it was not possible to attain equivalent strengths to those of the stronger precipitation hardened or cast alloys. [6,29].

Continued investigations into ODS aluminum-based systems led to further advancements. One of the more promising was that of the development of the IncoMAP alloys and similar Al-Li-Mg alloys.[30-32] Both offer an attractive combination of low density and high strength. These alloys exhibit yield strengths of 350-450 MPa.[30-32] However, due to their low ductility and fracture toughness, they have proven to be commercially unacceptable.[33]

Rapidly Solidified Alloy Systems

Among the other approaches geared at the development of more stable Al-based alloys for elevated temperature applications, rapid solidification processing (RSP) received a considerable amount of attention.[8,18,34,35] Specifically, RSP research has been focused on aluminum alloys with solute additions of elements with either low solubility and/or low diffusivity in order to reduce the transformation and coarsening of the reinforcing particles at elevated temperatures, thus retaining the desired microstructure and mechanical properties.[36] The strength of RSP aluminum alloys is dependent on the size and distribution of reinforcing particles; this can be expressed by the temperature dependent Orowan equation:

$$\tau(T) = 0.8G(T)b/l + (f^{1/2}/b^3)\{Q_D + kTLn[(\varepsilon s^2/2\rho b^4 \nu_D)]\}$$ [34,37,38]

where:

$\tau(T)$:	Temperature dependent Orowan flow stress
$G(T)$:	Shear modulus of matrix at temperature T
b:	Burgers vector of dislocation
l:	Particle spacing
Q_D:	Activation energy for Diffusion controlled climb
ε:	Strain rate
f:	Particle volume fraction
s:	Obstacle climb distance
ρ:	Dislocation density
ν_D:	Debye frequency

From examination of the above equation, it can be seen that high strength RSP alloys can be achieved by obtaining a microstructure with a large volume fraction of fine particles. Specifically, it can be shown that favorable properties can be achieved with a distribution of particles ~10 nm in diameter, and a particle

spacing of ~20 nm, which is approximately equivalent to a volume fraction of 25%.

History of Rapid Solidification of Aluminum Alloys

Various RSP techniques have been employed to process a wide variety of compositions.[4,8,9,34,35,39-41] Powder metallurgy (P/M), spray forming, and melt spinning RSP techniques are three of the processing methods which have received a considerable amount of attention in the research community in recent decades. Progress with these RSP methods, as well as others, has increased the range of possible microstructures which can be achieved in comparison to those obtained by conventional means. For example, RSP methods offer means of grain refinement, extension of solid solubility, the production of fine, uniformly distributed precipitates and the formation of metastable crystalline and amorphous phases.[8,24,34-36,42,43]

The Al-Si-Fe-V, Al-Fe-Zr , and Al-Fe-Mn systems are three examples of alloy systems which have received attention and where considerable progress has been made.[9,39,44-46] Fine dispersions of intermetallics at sufficient volume fractions were attained in each of the alloy systems via RSP techniques attributing to favorable hardness and yield strength. The systems, however, failed to retain their mechanical properties at elevated temperatures.[9,45]

Powder metallurgy

The basic process of P/M RSP techniques can be described as a process that begins with the atomization of an alloy composition into fine powders. It is in this initial stage, where the molten charge is rapidly solidified into fine powders, in which unique microstructures can be obtained.[8,47] The atomization is followed by

a screening process to remove oversize particles, blending of the powders to homogenize the size distribution, loading the powder into containers, vacuum degassing, sealing the powders into containers, and finally full consolidation via hot isostactic pressing and extrusion (Figure 2.3).[8,47]

Spray forming

In an attempt to decrease the costs associated with the powder metallurgy and melt spinning techniques yet still achieve the unique microstructures, spray forming processes have been investigated.[48] Spray forming can be described as the atomization of a molten stream onto a rotating substrate, as shown in Figure 2.4. [49] The substrate in addition to rotating, also withdraws away from the atomization nozzle along the axis of the powder spray as the atomization process deposits material onto it, thus building up a three dimensional ingot of the desired alloy under RSP conditions. The RSP ingot is then forged and machined to final shape, eliminating several of the consolidation steps necessary in P/M.

Properties

Although the properties of aluminum alloys have been extended beyond those of a number of conventional aluminum alloys by RSP techniques, they have yet to meet the challenge of developing an aluminum alloy which maintains its mechanical properties at elevated temperatures.[9,18] Figure 2.5 illustrates the typical decrease in the yield strength due to exposure to elevated temperatures for some Al-Fe-based RSP alloys.[9] Investigations of the mechanical properties and elevated temperature properties of Al-Fe-V-Si RSP alloys have yielded similar, more promising results (Figure 2.6).[44] Microstructures consisting of 24%

volume fraction of intermetallics were achieved via RSP processing of Al-Fe-V-Si alloys and exhibited maximum yield strengths of 525 MPa. Their properties, however, also deteriorate at temperatures at or above 150°C due to particle coarsening.[44] The 2219 wrought aluminum alloy, in comparison to RSP alloys, has much lower maximum yield strength of ~310 MPa, but maintains up to 93% of its room temperature strength up to 150°C.[5] A similar argument can be made in the case of the cast Al-Si based alloys in comparison to the RSP and wrought alloys. The cast alloys have much lower strengths overall, but are much better in retaining their strength at mildly elevated temperatures of 150-200°C. Though the strengths of several RSP alloys have been shown to match those of the higher strength conventional aluminum alloys, they still lack the desired elevated temperature performance. And since such RSP techniques are process intensive, they tend to be too expensive for most applications.[4]

Ternary Eutectic Systems

Although the application and development of binary eutectic systems are common and have been well studied,[49,50] only a limited body of knowledge exists concerning ternary eutectic systems due to the level of complexity of such systems.[51,52] Ternary eutectic growth processes which involve the nucleation and growth of three solid phases from the liquid is an attractive research topic within the materials science field.[11,12,53-56] Of specific interest are ternary eutectic systems which result in a cooperative solidification of all three phases, resulting in an in-situ composite consisting of the two intermetallic strengthening phases in a continuous matrix.[1,53,54,57-59] The effect of volume fraction on phase morphology has

been observed in several binary eutectic systems.[60] Specifically, as the volume fraction of the minor phase in eutectics decreases, a transition from a lamellar to a rod is observed.[60] Additionally, spherical intermetallics have been shown to form on solidification of binary systems comprised of low volume fractions of intermetallics.[61] However, at the volume fractions at which the spherical eutectic is formed, ~ 10% or less, the volume fraction is too low to have any significant strengthening. Considering this, it may be possible to obtain increased volume fractions of spherical strengthening phases by the solidification of a ternary eutectic system comprised of two binary eutectics both having low volume fractions of intermetallic phases. With the development of such microstructures, it is plausible that an alloy system could be designed with a sufficient volume fraction of the eutectic phases to achieve the desired mechanical properties. [62-65]

Under equilibrium solidification conditions of off-eutectic compositions, the formation of the eutectic structure will follow the nucleation and growth of a primary phase. However, previous work on binary eutectics has shown it may be possible to form the eutectic structure in some binary alloys under sufficient non-equilibrium solidification rates in off-eutectic compositions, thus allowing the possibility of alternating the volume fraction of the eutectic phases in the structures obtained, and making such investigations of ternary eutectics attractive.[42,43,57]

Bi-Cd-Sn System

The Bi-Cd-Sn ternary eutectic is a faceted/faceted/non-faceted system that forms microstructures comprised of three lamellar phases on solidification;

similar examples of eutectics which form three-phase microstructures on solidification include the Bi-In-Sn, and Bi-Cd-Pb systems.[59,66,67] Although each of the Bi-Cd-Sn, Bi-In-Sn, and Bi-Cd-Pb eutectics readily form a three-phase solid eutectic on solidification, it has been observed that the microstructures are not comprised of an intimate mixture of all three phases. Instead, however, the three systems display a strong tendency to form "double binary" regions in the microstructure, or regions where there are neighboring regions of two of the binary eutectics from the ternary system. Figure 2.7 gives an example of this in the Bi-In-Sn ternary, where regions of the BiIn-Sn and Bi-Sn binaries are seen adjacent to each other in the microstructure, instead of a homogeneous distribution of each of the three BiIn, Bi, and Sn phases in the microstructure.[66,67] These findings were consistent with previous predictions made by Smith concerning solidification of ternary eutectics, which suggest that it may not be possible to form an intimate mixture of three solid phases via eutectic solidification in systems that consist of two minor phases of lamellar morphology.[68] Smith, however, also predicted that in ternary eutectic systems it may be possible to obtain an intimate mixture of all three solid phases via eutectic solidification if one of the two minor phases solidified with a fibrous morphology.[68]

Al-Cu-Ni and Cd-In-Sn Systems

The Al-Cu-Ni and Cd-In-Sn are two examples in which a homogeneous distribution of the three phases can be obtained on solidification of a ternary eutectic.[11,56] In the case of the Al-Ni-Cu ternary eutectic cast via directional

solidification, the two minor phases in the α-aluminum matrix are θ-Al_2Cu and τ-Al_6Cu_3Ni, (Figure 2.8), and appear in the microstructure as faceted rods.[11] Likewise, in the case of the Cd-In-Sn ternary eutectic cast via directional solidification, the Cd and γ-Sn phases form as either broken lamellar or fibrous structures in the matrix of the In_3Sn phase.[56] Both of the Al-Cu-Ni and Cd-In-Sn ternary eutectics have at least one minor phase which forms with a rod morphology, and the formation of homogeneous distributions of phases in each of the systems is consistent with Smith's prediction concerning the solidification of ternary eutectics.[68]

Al-Ce-Ni System

Previous investigations of eutectics and the need for strong, lightweight structural materials focused more attention towards the development of aluminum-based alloys, and lead to the investigation of the Al-Ce-Ni system. An investigation by Belov and Naumova of the Al-Ce-Ni system lead to the discovery of a ternary eutectic at Al-12Ce-5Ni.[1] In development of the aluminum-rich portion of the ternary phase diagram (Figure 2.9), the microstructure obtained at the eutectic composition was comprised of a distribution of what was believed to be Al_4Ce and Al_3Ni intermetallics in an aluminum matrix. [1] The fully eutectic microstructures formed at the eutectic composition were also found to have a combined Al_4Ce and Al_3Ni volume fraction of approximately 25%, which was believed could lead to favorable mechanical properties if these phases were distributed uniformly.[1]

Belov and Naumova reported promising mechanical property results from their initial investigation. Hardness of the alloys cast was reported as a function of composition as well as hardness of ingots cast from the ternary eutectic composition after elevated temperature exposures. The hardness of the ternary system was shown to exceed 80 HB as the ternary eutectic composition was approached (Figure 2.10).[1] Thermal exposures of the eutectic composition at various elevated temperatures show a retention of hardness after 1 h exposures at temperatures of up to 400°C (Figure 2.11).[1] These properties suggest the possible application of this system, but it has yet to be further investigated.

Al-Ni and Al-Ce Binary Eutectic Systems

Previous researchers of the Al-Ni and Al-Ce binary systems observed fully eutectic microstructures at Al-5.7wt% Ni and Al-12wt% Ce, with volume fractions of intermetallics of approximately 8% and 15%, respectively.[13,57,69] Both binaries are of the faceted/non-faceted type and were observed to form eutectic microstructures at off-eutectic compositions with sufficient solidification rates.[13,14]

The stability of the Al-Ce and Al-Ni eutectic microstructures was investigated by Hawksworth and Nakagawa, respectively.[70,71] Though the minimum temperature resulting in microstructural coarsening was not reported, Hawksworth reported coarsening of the Al-Ce eutectic structure after exposures of 10 h or greater at 500°C.[70] Similarly, though the minimum temperature at which the Al-Ni eutectic microstructure coarsened was not published, Nakagawa and others reported coarsening of the Al-Ni eutectic at 525°C after 2 hour exposures.[72,73] While in both studies he authors reported observing coarsening of

the microstructures at high temperatures, they did not conduct an investigation concerning the minimum temperatures at which coarsening occurs.

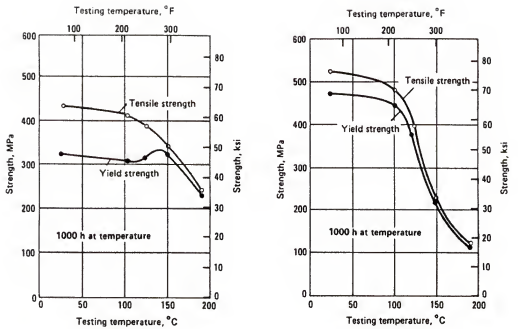

Figure 2.1 Plots of strength as a function of test temperature after 1000 hour soak at temperature for a) 2024-T3 and b) 7075-T6.[2]

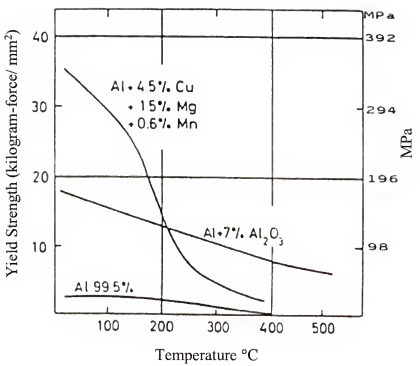

Figure 2.2 Yield strength as a function of test temperature for Al-4.5%Cu-1.5%Mg-0.6%Mn (2024-T3), Al+7vol% Al_2O_3, and pure aluminum.[2]

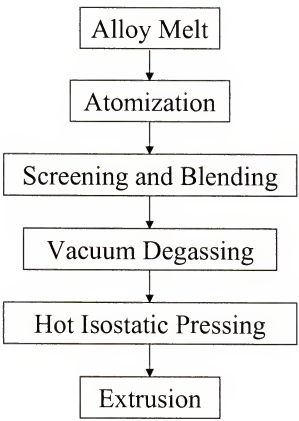

Figure 2.3 Schematic representation of P/M process for aluminum alloys.[7, 47]

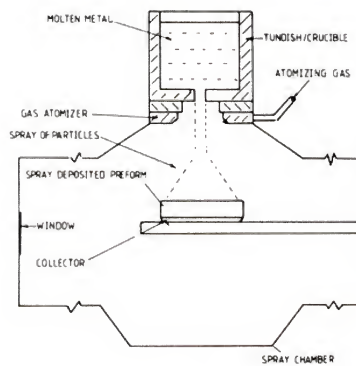

Figure 2.4 Schematic representation of spray forming process.[49]

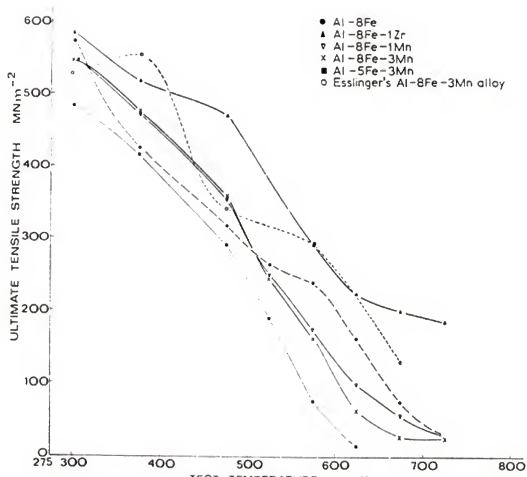

Figure 2.5 Yield strength as a function of test temperature for various Al-Fe-based RSP alloys after 100 hr exposure at test temperature.[8]

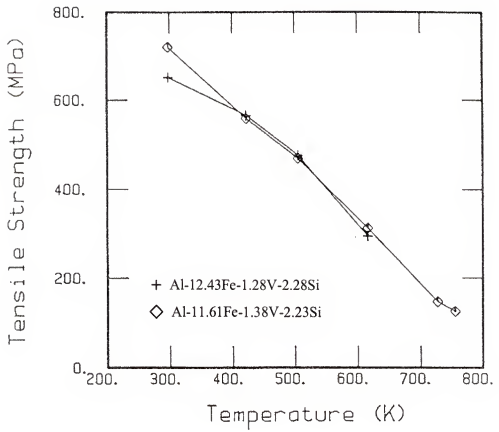

Figure 2.6 Tensile strength as a function of test temperature for Al-Fe-V-Si RSP alloys at test temperature [44]

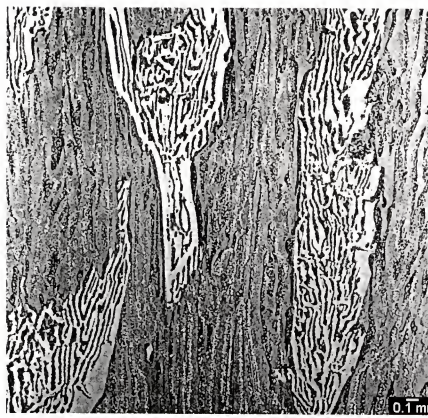

Figure 2.7 Backscattered electron image of longitudinal section of Bi-In-Sn ingot processed via unidirectional solidification, showing microstructure consisting of BiIn-Sn and Bi-Sn two phase regions in the ternary eutectic: Bi phase (white), BiIn phase (light gray), and γ-Sn phase (dark gray).[66,67]

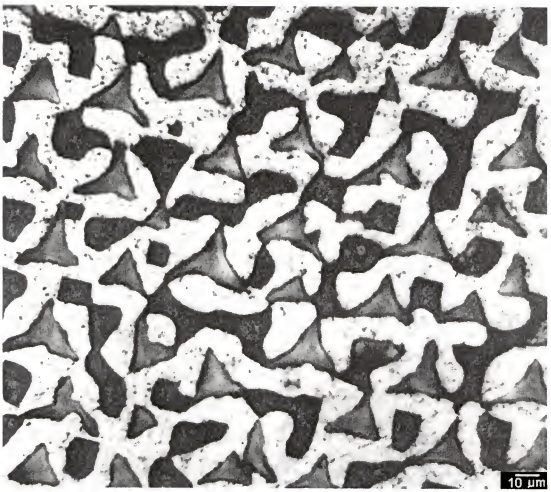

Figure 2.8 Optical micrographs of transverse section of Al-Ni-Cu ingot processed via unidirectional solidification, showing ternary eutectic microstructure: τ-Al_6Cu_3Ni phase (gray), θ-Al_2Cu phase (black), and α-aluminum (white).[56]

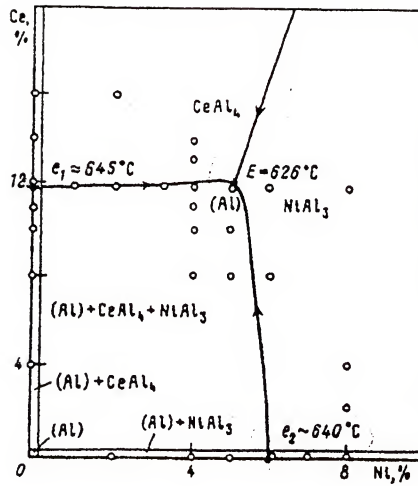

Figure 2.9 Projection of liquidus troughs in the aluminum rich corner of the Al-Ce-Ni ternary phase diagram, with ternary eutectic at Al-12Ce-5Ni (wt %). Circles represent compositions studied to generate diagram. [1]

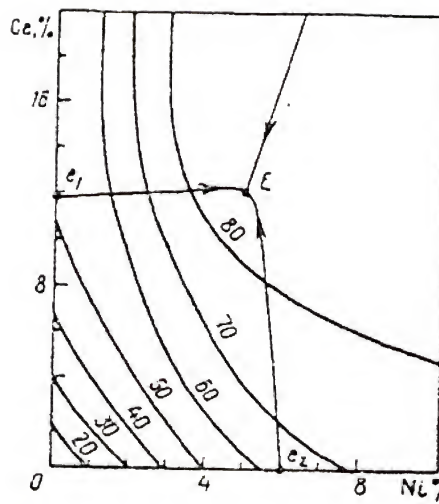

Figure 2.10 Hardness profiles (HB) of ternary alloys superimposed over aluminum rich corner of Al-Ce-Ni ternary phase diagram. [1]

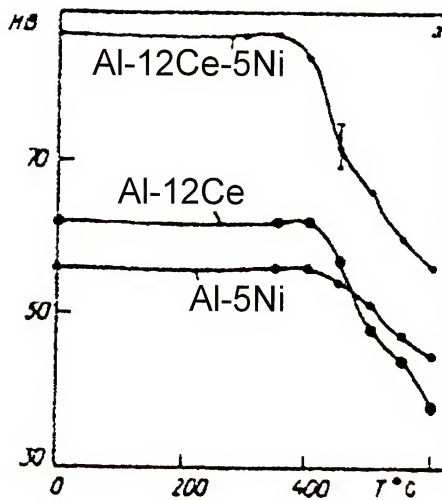

Figure 2.10 Room temperature hardness (HB) of the ternary Al-Ce-Ni eutectic composition as well as the two Al-Ce and Al-Ni binary eutectics after 1 hour at temperatures indicated. [1]

CHAPTER 3
SOLIDIFICATION MICROSTRUCTURE SELECTION OF THE ALUMINUM-NICKEL-CERIUM TERNARY EUTECTIC SYSTEM

Background

It has been well known for several years that alloys exhibit substantial changes in both phase distribution and microstructural morphology as the rate of solidification is altered. One of the earlier observations of this in a eutectic system was seen in the shift in the composition at which the eutectic could be formed in the Al-Fe system due to rapid solidification.[74] Similar observations have been made on other systems such as Al-Si, Ag-Al, Al-Ni, Al-Co, and Al-Cu.[57,75-77] Accompanying the shift in composition at which the eutectic structure forms, a corresponding shift in the volume fraction (*f*) of the eutectic phases is also observed.[78] These studies performed on the solidification of eutectic systems on the basis of composition and solidification rate have lead to the understanding of the coupled (or cooperative) growth in eutectics. The cooperative growth region was described as the range of compositions and solidification conditions which result in eutectic solidification without primary phase formation. The theory which describes this observation is based on diffusion controlled growth characteristics of eutectics and dendrites, where at off-eutectic compositions and sufficient solidification rates, due to the atomic attachment kinetics at the interface and diffusion kinetics, the eutectic structure forms at faster rates than that of the primary phases.[60,78]

In the case of binary eutectic systems consisting of two non-faceted phases, such as the Ag-Cu and Pb-Sn systems, the range of compositions and solidification conditions for cooperative growth has been shown to be symmetric about the eutectic composition (Figure 3.1a).[79] Alternatively, in the case of binary eutectics consisting of a faceted and a non-faceted phase such as the Al-Fe and Al-Si systems, the cooperative growth region is skewed towards the faceted phase (Figure 3.1b).[18,80-82] This can also be expressed as the ability to form the eutectic structure at hypereutectic compositions with sufficient solidification front velocity for faceted/non-faceted systems.

Solidification rate has also been observed to affect eutectic spacing. Jackson and Hunt concluded that, within the limits of stability for eutectic growth, there is an inverse relationship between solidification rate and eutectic spacing.[49] In addition to the changes in phase distribution and morphology observed as a function of solidification rate, shifts in solid solubility have also been observed as a function of solidification rate.[42,43,83]

Although substantial effort has been put forth towards the investigation of binary solidification microstructures, there still remains a lack of knowledge concerning the solidification behavior of ternary eutectic systems.[66,84] In view of this lack of knowledge of the solidification behavior of ternary eutectics, the present experiments were undertaken with the objective of providing insight into the effects of solidification rate on the microstructure of an Al-Ce-Ni ternary eutectic. For this study, a wedge mold casting technique was employed in which, due to the continuous change in ingot thickness in the wedge shaped ingot, it is

possible to observe the effects of various solidification rates on a single ingot casting.[58,85]

Experimental Work

Alloys consisting of 15-16 g charges were produced from high purity elements (99.9999% Al, 99.99% Ni, and 99.9% Ce) by a non-consumable electrode arc melting process. The aim compositions are listed in Table 3.1 and depicted on the Al-Ce-Ni phase diagram (Figure 3.2) starting with alloy composition 1, the ternary eutectic composition Al-12 wt% Ce-% 5 wt% Ni. Prior to arc melting, the chamber was evacuated to 10^{-2} Torr and flushed with argon to ~50 kPa. This cycle was repeated three times in succession to promote an oxygen depleted atmosphere. Titanium getters were then melted to remove ("getter") any remaining oxygen. Alloy buttons were then produced and these were turned over on the hearth a minimum of 5 times and remelted in an attempt to produce a homogeneous distribution of the elements throughout the button.

After alloying, each of the compositions was remelted in the arc melting chamber on a graphite crucible, under the same atmospheric conditions as in the initial melting, and cast into a wedge-shaped copper mold with a 15° angle, resulting in ingots with the following approximate dimensions: 10 mm wedge thickness, ~12 mm width, and ~45 mm height (Figures 3.3 and 3.4).

X-ray diffraction (XRD) was performed on various locations of each of the ingots using a Philips APD 3720 X-ray diffractometer. Experiments were performed between the angular limits of $10° < 2\theta < 90°$, using a Cu K_α source. Longitudinal sections of the ingots were made along the length of the wedge

shape, and ground and polished through 0.3 μm alumina for analysis via optical and scanning electron microscopy (SEM). SEM work was performed on either a JEOL 6400 or 6315F scanning electron microscope, and energy dispersive spectrometry (EDS) work on the SEM's accompanying Oxford microanalysis hardware with Link ISIS software package for compositional analysis. Transmission electron microscopy was also performed using a Philips EM 420 equipped with an EDAX 9800 EDS system. Samples for TEM analysis were prepared by initially thinning with SiC paper followed by jet polishing in a 1:2:7 solution of perchloric acid:ethylene glycol:methanol at –25°C, 30 mA, and 12 mV.

Results and Discussion

XRD experiments yielded characteristic peaks for α-aluminum, $Al_{11}Ce_3$ and Al_3Ni (Figure 3.5), but no other binary or ternary compounds. It should be note that the Al-Ce intermetallic is in fact $Al_{11}Ce_3$, not Al_4Ce as previously published by Belov and co-workers.[12] Results of the compositional analysis are listed in Table 3.2 and show that the cast compositions fall within 0.5 wt% of the nominal target compositions. Analysis of the longitudinal sections of the nine ingots revealed five distinct microstructural zones (I-V). These zones were found to be comprised of (I) primary α-aluminum dendrites and an interdendritic ternary lamellar microeutectic, (II) a fine cooperatire growth ternary microeutectic, (III) primary $Al_{11}Ce_3$ and ternary microeutectic, (IV) primary Al_3Ni and ternary microeutectic, and (V) primary $Al_{11}Ce_3$ and Al_3Ni, and microeutectic (Figure 3.6-3.10). Figure 3.11 illustrates the location of the microstructural regions in each of the ingots cast at the nine compositions.

The primary α-aluminum dendrites and interdendritic microeutectic (zone I) was characteristically found near the tip of the wedge mold and the extreme periphery of the mold edge, specifically in those regions associated with the highest cooling and solidification rate. The coupled growth microstructure (zone II) was characteristically observed at the intermediate regions of the wedge mold. Similarly, combinations of the primary $Al_{11}Ce_3$ and/or Al_3Ni, and eutectic (zones III, IV, and V) were observed at the widest regions of the wedge-cast ingot associated with the slowest cooling rate.

The interdendritic eutectic in zone I (α-Al + microeutectic) at the tip of the wedge castings is not as fine as that observed in the coupled growth eutectic structures (zone II), as seen in comparison of Figures 3.6 and 3.7. This may be caused by an increase in the volume fraction of the $Al_{11}Ce_3$ and Al_3Ni intermetallic phases in that region, resulting in coarser structures tending towards a distribution of more blocky phases instead of a fine eutectic structure. This is supported by EDAX analysis performed on the interdendritic regions of several of the Al-Ce-Ni wedge cast ingots, which reveals a higher concentration of both Ce and Ni with respect to the bulk composition, (Table 3.3). Das et al. have made similar observations in a study of Al-Ni alloys via laser surface melting.[86] Where instead of the α-Al + Al_3Ni eutectic in the Interdendritic regions, only plates of Al_3Ni were seen in the microstructure of the laser surface melted Al-Ni alloys processed at the highest speed and energy input. [86]

This increase in the intermetallic volume fraction in the interdendritic region may be caused by two factors. First, on solidification at the tip of the

wedge mold Ce and Ni are rejected into the liquid as the α-Al dendrites solidify. This shifts the liquid composition to higher solute compositions, as the Al is consumed by the advancing dendrites. The liquid composition will continue to enrich in solute content until the $Al_{11}Ce_3$ and Al_3Ni are undercooled a sufficient amount for nucleation, thus resulting in a shift of the interdrendritic microstructures towards higher Ce and Ni concentrations and volume fractions. Secondly, Gigliott et al. have shown that non-faceted phases act as poor nucleation sites for faceted phases.[87] In this case, the non-faceted primary Al dendrites, act as poor nucleation sites for the $Al_{11}Ce_3$ or Al_3Ni, thus also driving the interdendritic liquid to higher solute concentrations prior to nucleation of the Interdendritic eutectic.

Small regions of α-Al was also observed on the periphery of primary intermetallic phases in zones III, IV, and V, as shown in Figures 3.8 - 3.10. Halos of non-faceting phases have been observed to form about primary faceting phases in hypereutectic compositions of binary eutectics of the faceted/non-facetted type.[82,87-90] Formation of halos such as these has been explained in terms of solute diffusion and growth velocities of the phases involved.[87,89,90] In previous work performed on hypereutectic Al-Si compositions, Yilmaz et al. as well as Barclay et al. proposed that upon solidification of hypereutectic compositions, the primary faceted phase will nucleate at some temperature T_o, just below the liquidus temperature predicted by the equilibrium phase diagram for the given composition C_o (Figure 3.16).[88,90] With continued solidification and further primary phase formation, the mean liquid composition will decrease, following a

depressed liquidus curve (Figure 3.16).[88,90] However, Yilmaz et al. and Barclay et al. proposed that, as the Si is consumed by the advancing primary phase, there is an enrichment of Al in the liquid immediately adjacent to the primary phases.[88,90] As the liquid reaches the Al-Si eutectic composition, the growth velocity of the α-Al phase from the aluminum-rich periphery of the primary phase is greater than that of Si solute diffusion into the aluminum-rich region. This drives the α-Al formation at the periphery of the primary phase, prior to the solidification of the eutectic structure.

Similar to halo formation in the binary eutectic system, in hypereutectic compositions of the Al-Ce-Ni system, as the primary $Al_{11}Ce_3$ and/or Al_3Ni phases solidify, Ce and/or Ni is depleted from the melt, shifting the liquid composition towards the ternary eutectic as the liquid composition follows the depressed ternary liquidus. As in the case of halo formation in the Al-Si system, as the liquid reaches the ternary eutectic composition, the growth velocity of the α-Al phase from the aluminum-rich periphery of the primary phase is greater than that of Ce and Ni solute diffusion. Thus results in the formation of α-Al at the periphery of the primary phase prior to the solidification of the ternary eutectic structure.

Kiminami et al. developed a model which describes the cooling rate of the ingots cast in the copper wedge mold as a function of alloy composition and mold geometry (Figure 3.12).[91] Application of this model in comparison to the microstructures obtained from casting of the various compositions in this study has been used to describe the general shape of the cooperative growth region for the ternary eutectic. Examination of the microstructures from the cast

compositions 1, 2, and 5 suggest that, as the cerium concentration is increased from the ternary eutectic composition, the cooperative growth region is skewed towards the faceted phase, as in classical faceted/non-faceted binary eutectics, (Figure 3.13). Similarly, examination of the microstructures in ingots cast from compositions 1, 3, and 6 reveal the same phenomena for increasing nickel concentration, but within a narrower range of cooling rates (Figure 3.14). At compositions at which both the nickel and cerium concentrations increase with respect to the ternary eutectic (compositions 4 and 7), the same phenomena of the cooperative growth region skewed towards the faceted phases is observed, (Figure 3.15). In the case of the microstructures solidified from composition 7, however, a unique observation can be made. Although both the primary $Al_{11}Ce_3$ and Al_3Ni intermetallics are observed at the widest section of the wedge (regions associated with the slowest cooling rates), the primary Al_3Ni was observed in lower sections of the ingot in comparison to that of the $Al_{11}Ce_3$. This corresponds to the formation of the primary Al_3Ni at greater cooling rates to that of primary $Al_{11}Ce_3$, or the formation of the primary Al_3Ni at a faster rate compared to $Al_{11}Ce_3$.

TEM foils were also prepared and examined. Viewing the structure at significant magnifications in the TEM, reveals a unique, chain-like array of alternating intermetallics (Figure 3.17a). Bright field images obtained perpendicular to the length of the intermetallics illustrate the rod shape of the $Al_{11}Ce_3$ intermetallics and the spherical and/or low aspect ratio rods of Al_3Ni. Bright field/dark field (BF/DF) pairs suggest that each of the $Al_{11}Ce_3$ intermetallics

within the chain like microstructure is aligned in a similar orientation within the aluminum matrix (Figure 3.17c). Similarly, dark field images generated using Al_3Ni reflections, suggest that the Al_3Ni intermetallics in the chain like structures are also aligned along the same orientation with the microstructure (Figure 3.17d). Due to challenges in TEM analysis associated with the fine scale of the microstructure, the specific orientation relationships between the intermetallics and the matrix could not be completely determined with the as-cast microstructure. However, the characterization of the crystallography will be addressed in later chapters.

Conclusions

The Al-12wt% Ce-5wt% Ni ternary eutectic composition as well as 8 additional hypereutectic compositions were cast into a copper wedge mold to investigate their microstructural formation as a function of location (i.e., cooling rate). The ternary eutectic microstructure has been observed to form at hypereutectic compositions similar to the cooperative growth phenomena observed in binary eutectic faceted/non-faceted eutectics. At the highest nickel and cerium concentrations, the primary Al_3Ni was observed to form at higher cooling rates than $Al_{11}Ce_3$, suggesting it has faster growth kinetics. A unique microstructure in these structures was observed, and found to be comprised of chain-like structures of alternating $Al_{11}Ce_3$ and Al_3Ni intermetallics.

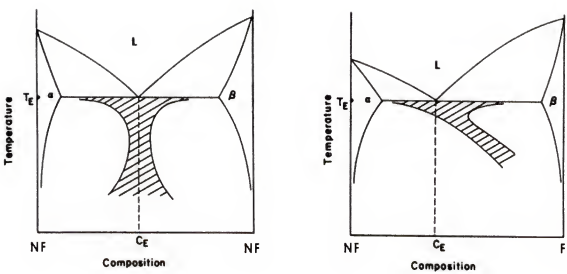

Figure 3.1 Cooperative growth regions for a) non-faceted/non-faceted and b) non-faceted/faceted binary eutectics.[78]

Table 3.1 Nominal compositions of Al-Ce-Ni alloys investigated (weight %).

Alloy #	Al	Ce	Ni
1	83	12	5
2	82	13	5
3	82	12	6
4	81	13	6
5	81	14	5
6	81	12	7
7	79	14	7
8	80	14	6
9	80	13	7

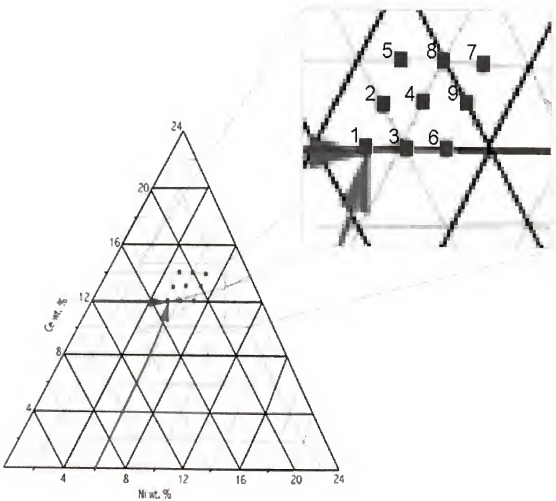

Figure 3.2 Nominal compositions of the Al-Ce-Ni alloys investigated, represented on the Al-rich corner of the Al-Ce-Ni ternary diagram, within the α-Al, $Al_{11}Ce_3$, Al_3Ni 3-phase field.

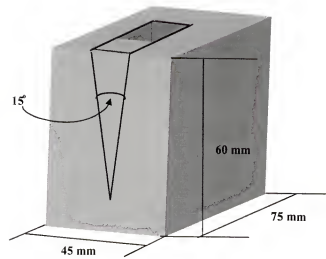

a)

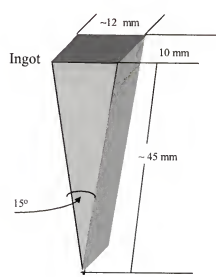

b)

Figure 3.3 Schematic of a) copper chill mold utilized in wedge mold castings, and b) approximate dimensions of resulting ingots.

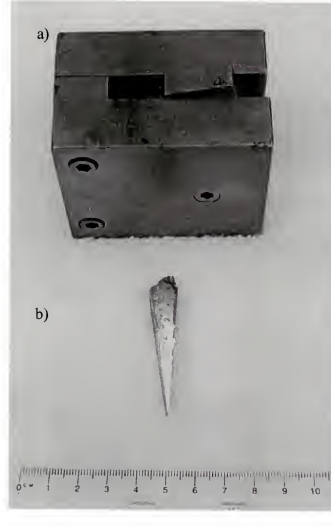

Figure 3.4 Photo of a) wedge mold used in experimentation and b) representative resulting ingot.

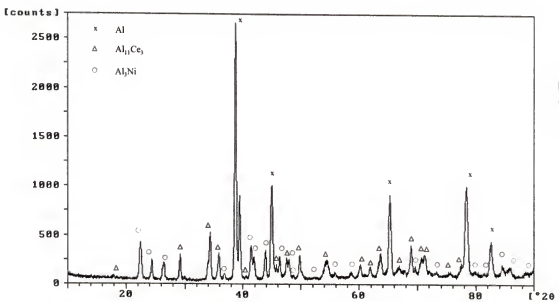

Figure 3.5 Representative XRD results for cast ingots showing only α-aluminum, $Al_{11}Ce_3$, and Al_3Ni phases.

Table 3.2 Empirically Determined Compositions of Al-Ce-Ni alloys investigated (weight %).

Alloy #	Al	Ce	Ni
1	83.3	11.6	5.0
2	82.6	12.5	4.7
3	82.0	11.8	6.0
4	81.0	13.1	5.7
5	81.3	13.8	4.7
6	81.3	11.8	6.6
7	79.4	13.7	6.6
8	80.3	13.7	5.8
9	80.4	12.8	6.7

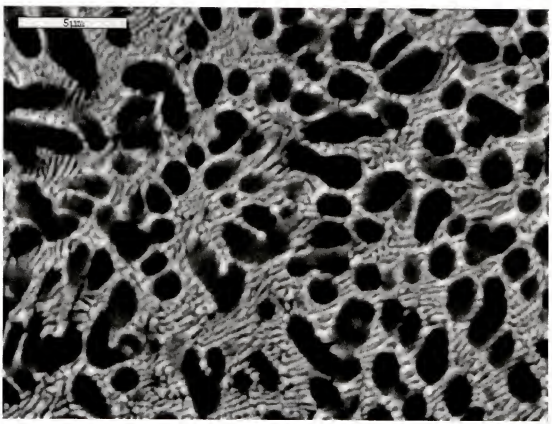

Figure 3.6 BSE image of zone I microstructure consisting of primary α-aluminum dendrites (dark) and lamellar interdendritic microeutectic (α-Al + $Al_{11}Ce_3$ + Al_3Ni).

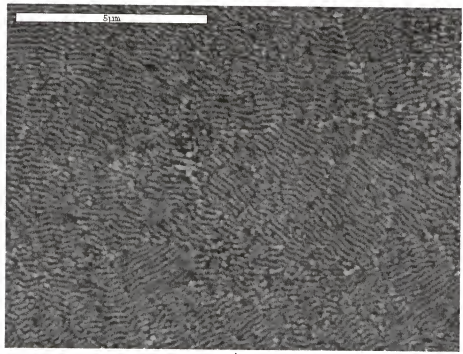

a)

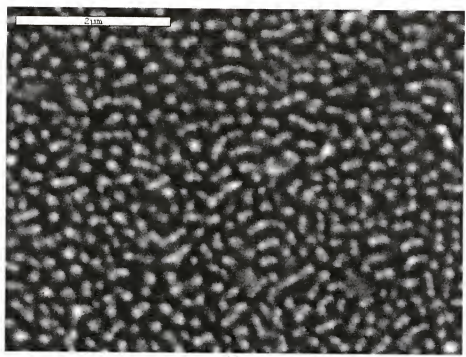

b)

Figure 3.7 BSE images of a) zone II microstructure consisting of fine cooperative growth ternary eutectic. b) higher magnification of cooperative growth region revealing unique chain-like structure of alternating $Al_{11}Ce_3$ (bright) and Al_3Ni (gray) intermetallic phases in aluminum matrix (dark).

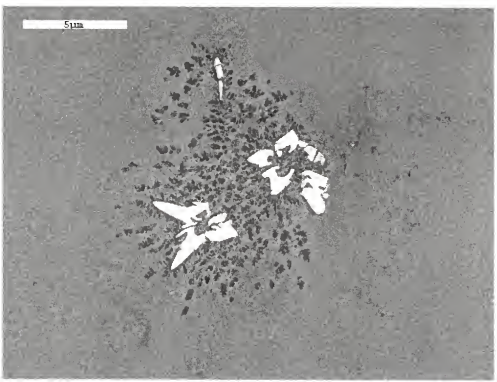

Figure 3.8 BSE image of zone III microstructure consisting of primary $Al_{11}Ce_3$ (white) surrounded by halos of α-Al (dark gray) at the periphery of the intermetallic and cooperative growth eutectic.

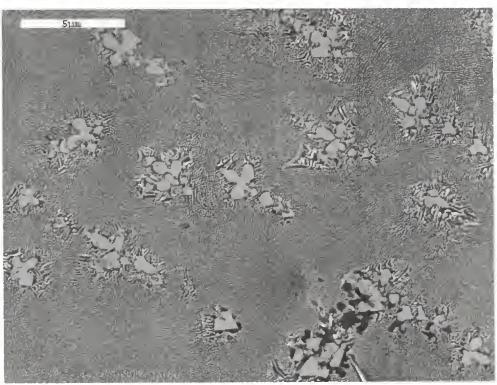

Figure 3.9 BSE image of zone IV microstructure consisting of primary Al_3Ni (gray), surrounded by ternary eutectic.

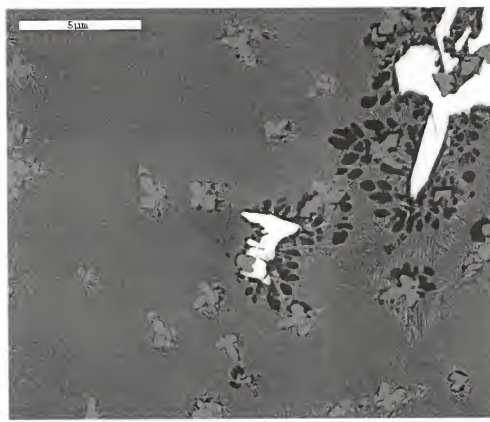

Figure 3.10 BSE image of zone V microstructure consisting of primary Al_3Ni (gray), $Al_{11}Ce_3$ (white) surrounded by the eutectic.

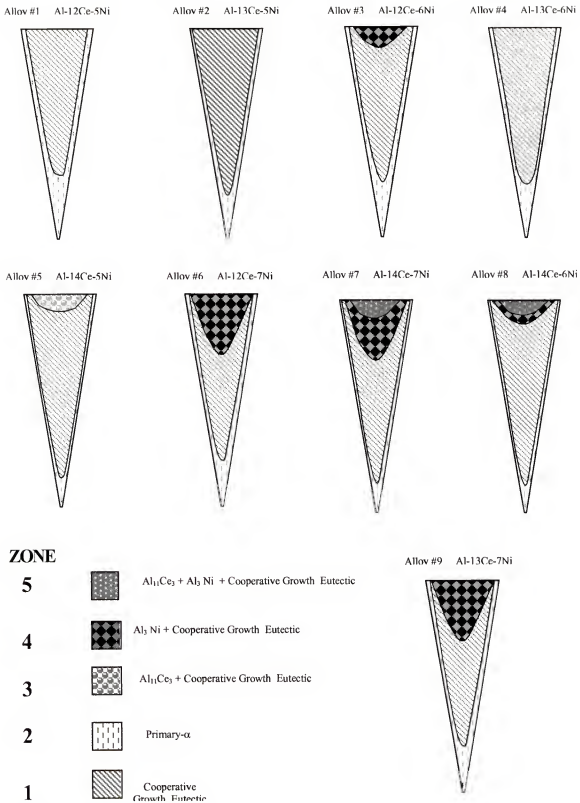

Figure 3.11 Schematic representation of the microstructural zones in each of the compositions cast into wedge molds.

Table 3.3 Empirically Determined Bulk Compositions and Compositions of Interdendritic Regions of Various Al-Ce-Ni alloys investigated (weight %).

	Bulk Composition			Interdendritic Composition		
Alloy #	Al	Ce	Ni	Al	Ce	Ni
1	83.3	11.6	5.0	73.9	18.2	7.9
2	82.6	12.5	4.7	61.8	27.8	11.6
3	82.0	11.8	6.0	55.6	29.1	15.3

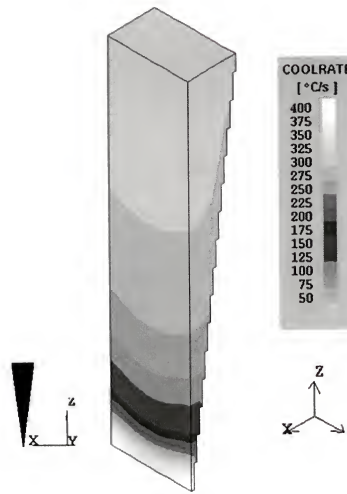

Figure 3.12 Model of temperature profile sectioned from the center of a wedge mold casting.[91]

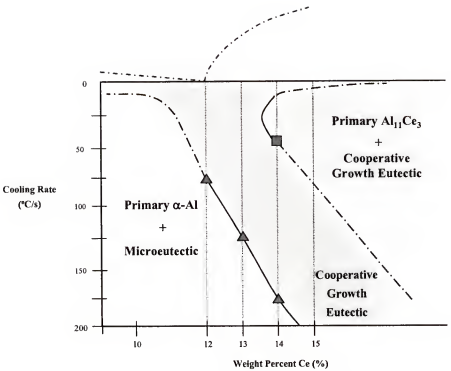

Figure 3.13 Cooperative growth region shown within an isopleth of constant nickel concentration of 5wt%, for compositions starting at the eutectic composition, with increasing cerium (ie., alloys 1, 2, and 5).

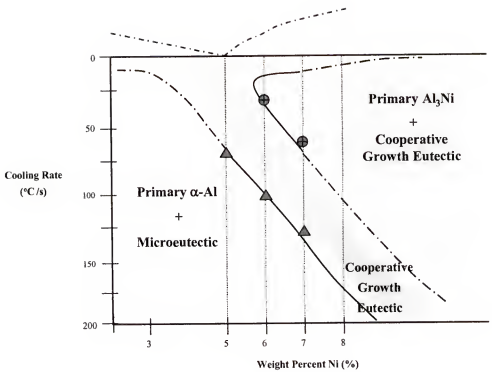

Figure 3.14 Cooperative growth region shown within an isopleth of constant cerium concentration of 12 wt%, for compositions starting at the eutectic composition, with increasing nickel (ie., alloys 1, 3 and, 6).

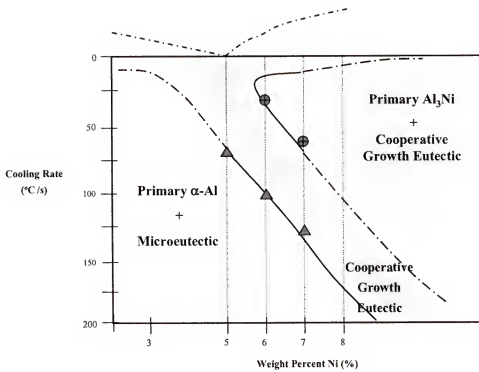

Figure 3.15 Cooperative growth region shown within an isopleth starting from the eutectic composition to those with linear increases in both cerium and nickel concentrations (ie., alloys 1, 4 and, 7).

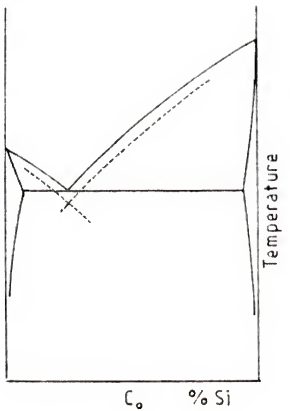

Figure 3.16 Al-Si binary phase diagram. Dashed lines below equilibrium liquidus lines represent local equilibrium concentration of liquid adjacent to primary phase as a result of non-equilibrium solidification.[90]

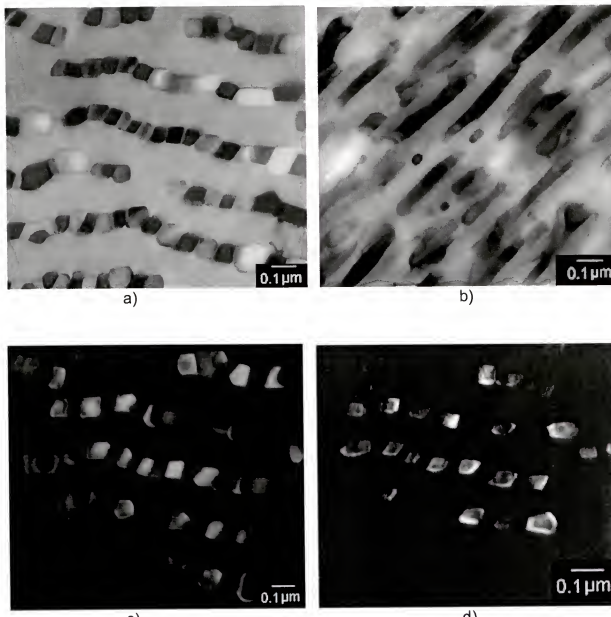

Figure 3.17 TEM images of a) BF with a chain like structure consisting of dark gray $Al_{11}Ce_3$, strongly diffracting intermetallics and gray Al_3Ni intermetallics in an aluminum matrix, b) BF image of illustrating rod like nature of $Al_{11}Ce_3$ and more spherical nature of Al_3Ni intermetallics c) DF of same field as above BF (a) showing similar orientation of $Al_{11}Ce_3$ intermetallics, d) DF of same field as above BF showing similar orientation of Al_3Ni intermetallics.

CHAPTER 4
ELEVATED TEMPERATURE STABILITY OF ALUMINUM-CERIUM-NICKEL TERNARY EUTECTIC STRUCTURES

Background

The application of structural materials for elevated temperature service is often limited by microstructural stability. In the case of precipitation strengthened and many RSP structural aluminum based alloys, the instability is often evident as a coarsening or dissolution of the strengthening phases, which is accompanied by a loss in strength. The inability of precipitation strengthened and RSP alloys to sustain strength at elevated temperatures has been observed by several investigators.[7-9,18,92] A possible means of addressing the need for lightweight structural materials is in the design of microstructures consisting of stable, equilibrium, strengthening particles formed from the melt, thus tending to greater thermal stability.[93] The Ti-TiB eutectic has been explored for service at temperatures approaching 600°C, with only moderate success due to challenges arising from a the low volume fraction (~8%) of the TiB strengthening phase in the eutectic.[93] Similarly, the Ti-Ti_5Si_3 system has also been explored for similar service conditions, but due to difficulty in refining the faceted Ti_5Si_3 phase, sufficient strength has not been achieved.[93] Concerning aluminum-based alloy systems for slightly lower elevated temperature service, the Al-Al_2Cu and Al-Al_3Ni binary eutectic systems display favorable microstructural stability and strength retention at elevated temperatures.[71,73,94] Investigators have shown that Al-Al_3Ni

structures exhibit tensile strengths up to 350 MPa, with microstructures that were shown to have coarsened considerably after 2 h exposures at 500°C.[73] Similar findings were reported by Kraft and Graham in the investigation of the Al-Al_2Cu eutectic system, with the Al_2Cu intermetallic coarsening rapidly at 500°C.[94,95] Though there has been considerable effort in the investigation of such binaries for elevated temperature service,[71,73,94] there still remains a lack of information concerning the performance of ternary eutectics (as discussed in previous chapters). This chapter will explore the microstructural stability of the Al-12 wt% Ce-5 wt% Ni ternary eutectic as a function of elevated temperature exposure.

Experimental Work

Ten ingots of the Al-12 wt% Ce-5 wt% Ni ternary eutectic composition were prepared by casting into the copper wedge mold as described in the previous chapter. For the scope of this study, only the fine ternary eutectic microstructure is of interest in terms of obtaining optimum properties for structural applications, therefore off-eutectic compositions were not investigated. Ingots were sectioned and polished through 0.3 μm alumina. The fully eutectic microstructure was verified via SEM. Likewise, the compositions of the ingots were verified via energy dispersive X-ray spectroscopy (EDS). Samples were then encapsulated in quartz ampoules which were evacuated to 10^{-2} Torr and backfilled with high purity argon to –50 kPa before encapsulation. Microhardness tests were performed on the samples using a Buehler Micromet II Microhardness tester with a Vickers indenter and a 500g load. X-ray diffraction analyses were performed prior to and after elevated temperature exposures using a Philips APD

3720 X-ray diffractometer. XRD experiments were performed between the angular limits of $10° < 2\theta < 90°$, using a Cu K_α source. Heat treatment of the samples was performed per series of time and temperature profiles which consisted of exposure at 350°C, 400°C, 450°C, 500°C, or 550°C for either 1, 10, or 100 h; this was followed by SEM evaluation of the microstructures using either a JEOL 6400 or 6315F SEM. EDS analysis was performed using Oxford microanalysis hardware with Link ISIS software.

Results and Discussion

Results of the compositional analysis performed on the ten samples via EDS indicated that the compositions were within 0.5 wt% of the Al-12Ce-5Ni target eutectic composition. XRD analysis of ternary eutectic microstructures prior to heat treatment revealed only the α-aluminum, $Al_{11}Ce_3$ and Al_3Ni phases (Figure 4.1). Similarly, XRD performed after all heat treatments revealed no new phases (Figure 4.2). Results from microhardness tests performed on the ternary eutectic ingots after heat treatment are listed in Table 4.1, and show a substantial drop in hardness at exposures greater than 400°C (Figure 4.3). The fine as-cast microstructure of chains of alternating $Al_{11}Ce_3/Al_3Ni/Al_{11}Ce_3$ intermetallics, described in Chapter 2, is shown in Figure 4.4. SEM of the samples after thermal exposure shows a definite change in the ternary eutectic microstructure. Examination of the samples heat treated at 450°C for 1, 10, and 100 hours, respectively, illustrate the initial fragmentation of the fine ternary eutectic followed by coarsening (Figures 4.5-4.7). Accelerated coarsening was also observed at eutectic grain boundaries (Figure 4.8).

The XRD results are consistent with the observation that the properties of the as-cast material are a function of the coarsening of the microstructure due to thermal exposure, not the result of the formation of other binary or ternary phases at elevated temperatures. Thus, the decrease in hardness of the eutectic alloys is directly attributed to the coarsening of the constituent phases in the microstructure as a function of elevated temperature exposure; this is consistent with similar findings concerning the elevated temperature performance of the similar binary systems.[71,73,94] Coarsening within the grains of the eutectic is shown to occur initially by the fragmentation of the intermetallics after a one hour exposure at 450°C (Figure 4.4). Fragmentation, such as that observed in the Al-Ce-Ni ternary eutectic microstructure, has also been observed by Smartt et al. in previous studies rod eutectics.[73] Smartt et al. proposed that this fragmentation occurs at the initial stage of Ostwald ripening in which the principle diffusion pathway is perpendicular to the rod length, resulting in a shortening of the fibers or a "pinch-off" of the fibers, as shown in Figure 4.9.[73] This is followed by further coarsening of these fragmented particles due to continued exposure at this temperature (Figures 4.5-4.7). Throughout the coarsening process, the intermetallic spacing increases with a corresponding decrease in mechanical properties. A similar, but accelerated coarsening sequence was observed above 450°C, as expected. In comparison to the performance of the directionally solidified Al-Ni binary eutectic, studies by Bayles et al. have shown the binary eutectic exhibits microstructural stability at temperatures up to 572°C for exposure times of 138 h.[72]

Figures 4.4-4.7 and 4.8 suggest that the overall coarsening of the eutectic structure occurs by multiple mechanisms. First, within the eutectic grains, after initial fragmentation of the intermetallics, coarsening occurs via second phase coarsening or Ostwald ripening.[96,97] Secondly, accelerated coarsening is observed at the grain boundaries, due to the higher diffusivity there.[26,98]

Conclusions

The thermal stability of the Al-Ce-Ni ternary eutectic was investigated by heat treating the as-cast microstructure at various elevated temperatures for exposure times of 1, 10, or 100 hours. The intermetallics formed on solidification of the Al-12wt% Ce-5wt% Ni eutectic proved to be the equilibrium phases, which did not transform to other phases after extended thermal exposures of up to 100 hours at 550°C. The microstructure however did prove to coarsen from its original fine as-cast structure at exposures of over an hour at temperatures greater than 400°C. In these cases, the chain-like structure of alternating $Al_{11}Ce_3/Al_3Ni/Al_{11}Ce_3$ intermetallics was observed to fragment and then coarsen via a classic Ostwald ripening mechanism. Accompanying the coarsening of the microstructure, was a corresponding decrease in the hardness. The coarsening of the microstructure was found to occur via: a) classic Ostwald ripening of the intermetallics within the eutectic grains, as mentioned previously, and b) an accelerated coarsening at the grain boundaries due to the increased diffusion at the boundaries.

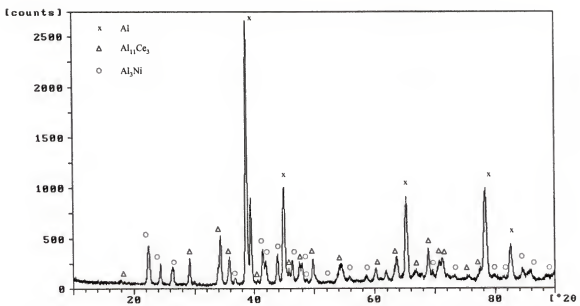

Figure 4.1 Representative XRD results for eutectic as-cast ingot.

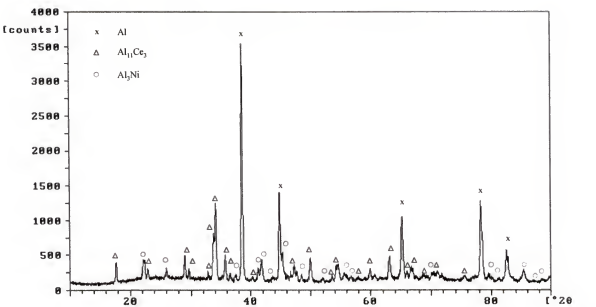

Figure 4.2 Representative XRD results for eutectic ingot after 100 hours at 500°C.

Table 4.1 Post Heat Treatment Microhardness Data

Heat Treat Condition	350 1Hr	350 10Hr	350 100Hr	400 1Hr	400 10Hr	400 100Hr	450C 1Hr	450C 10Hr	450C 100Hr	500C 1Hr	500C 10Hr	500C 100Hr	550C 1Hr	550C 10Hr	550C 100Hr
	119.7	120.4	114.4	117.3	112.5	111.3	86.5	98.0	68.3	81.0	78.4	68.6	76.1	65.5	60.8
	109.5	114.4	111.9	116.3	115.2	118.8	89.1	91.8	72.3	84.1	81.7	69.6	76.3	64.4	61.3
	118.3	107.2	111.9	116.8	119.6	115.1	87.0	92.2	77.0	90.0	78.0	71.8	75.2	63.7	59.1
	113.2	106.0	107.2	110.5	116.5	113.8	92.2	93.2	79.5	90.2	78.0	72.6	81.0	51.2	62.0
	110.5	114.4	104.9	115.4	117.9	117.7	86.2	91.3	81.4	87.2	78.0	71.3	84.1	51.6	58.6
	108.4	119.4	117.4	108.8	118.9	114.8	92.3	91.7	69.9	83.8	76.9	71.2	85.9	62.4	60.7
	111.3	120.1	114.7	118.1	117.4	113.8	87.9	95.7	78.1	87.3	77.2	70.5	77.7	64.0	64.8
	118.4	117.4	120.2	118.8	111.0	118.3	91.4	93.7	83.9	82.4	83.9	71.0	74.9	52.9	61.3
	110.3	119.3	119.5	119.0	118.4	110.3	91.7	92.9	69.0	83.0	79.2	68.9	77.4	55.3	57.7
	107.5	118.6	110.2	111.9	115.3	117.3	90.3	96.8	85.3	89.2	80.6	71.8	81.4	61.1	59.3
	118.2	118.0	109.2	117.6	118.9	109.9	91.9	93.8	80.2	90.1	82.8	70.8	83.6	63.7	57.2
	112.5	117.3	113.5	120.3	116.8	115.7	92.3	93.1	68.2	82.4	81.2	72.0	77.0	58.3	62.4
	109.3	119.9	118.2	118.3	117.0	119.3	89.0	92.8	78.1	90.0	78.3	70.0	78.9	62.1	60.4
	110.9	120.3	120.2	117.5	116.3	118.8	91.7	95.7	79.3	87.3	81.0	69.2	78.1	57.8	58.4
	109.9	119.9	120.3	120.6	113.6	113.0	90.8	97.4	77.0	87.3	81.1	71.6	82.5	55.9	61.8
	112.4	110.2	110.9	118.9	109.3	114.7	89.6	93.1	68.9	87.2	78.5	72.0	83.9	65.9	59.9
	110.3	117.9	119.9	117.4	120.5	118.7	91.5	91.2	74.9	87.2	79.5	70.5	84.7	62.8	58.2
	118.5	119.3	117.3	119.2	116.3	108.4	90.4	94.2	78.3	90.3	77.9	68.1	77.8	53.6	59.5
	110.3	120.1	118.3	119.1	117.8	114.0	91.3	94.1	80.2	88.3	80.7	70.9	79.5	61.5	62.4
	111.3	118.8	120.3	118.4	116.6	118.2	92.3	93.8	74.3	89.2	78.4	71.7	80.4	57.9	63.0
	112.8	119.6	119.4	114.8	112.6	112.9	91.4	94.1	79.4	89.2	79.4	70.1	75.3	59.1	64.9
	110.5	118.4	118.2	118.8	119.8	115.6	89.4	92.5	73.7	89.3	77.8	69.3	82.9	61.9	59.3
	117.4	118.3	119.3	120.1	119.6	114.9	90.4	92.1	74.3	85.6	76.4	71.9	77.3	58.9	62.1
	111.3	120.1	119.9	118.9	116.0	118.3	92.5	97.8	68.3	87.4	82.1	70.3	81.3	58.3	57.7
Average	111.0	112.0	110.0	111.0	111.0	115.0	89.0	93.2	76.0	87.0	79.0	71.0	79.0	60.0	60.9

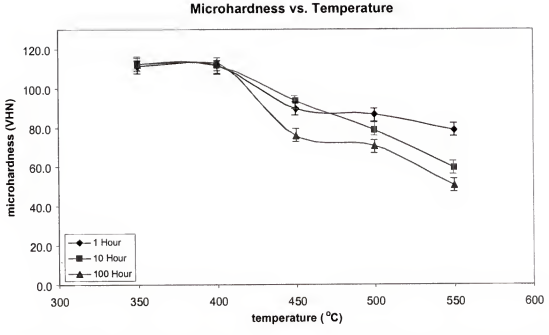

Figure 4.3 Microhardness of samples cast from the eutectic composition after elevated temperature exposure.

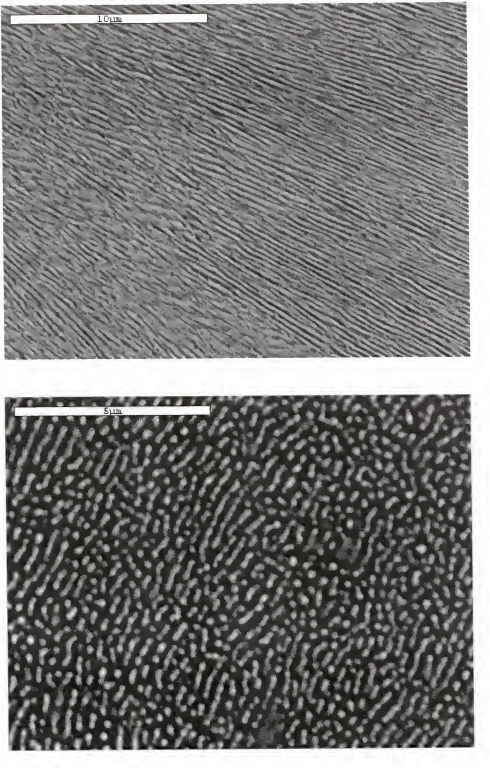

Figure 4.4 BSE images-of as-cast ternary eutectic microstructure comprised of alternating $Al_{11}Ce_3/Al_3Ni/Al_{11}Ce_3$ intermetallics (light gray phase is the $Al_{11}Ce_3$ and the dark gray phase is the Al_3Ni intermetallic).

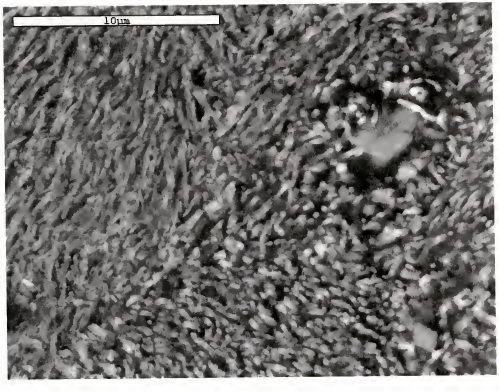

Figure 4.5 BSE image of eutectic microstructure after 1 hour at 450°C.

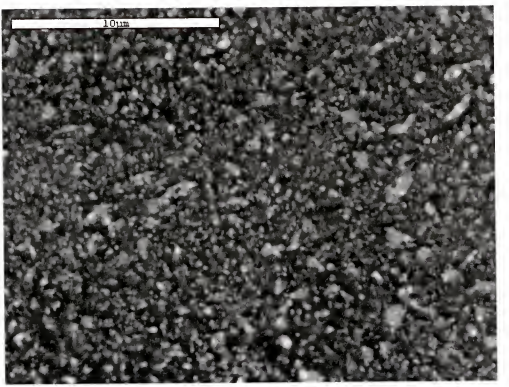

Figure 4.6 BSE image of eutectic microstructure after 10 hour at 450°C.

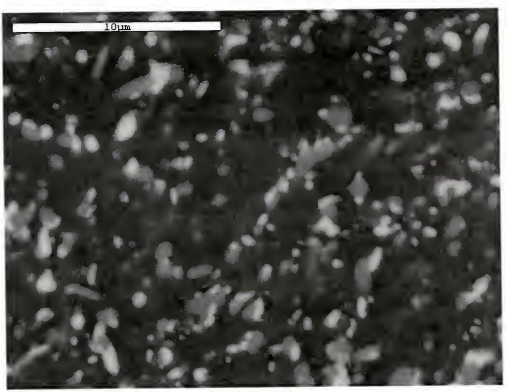

Figure 4.7 BSE image of microstructure after 100 hour at 450°C. After considerable coarsening distinct bright gray $Al_{11}Ce_3$ and dark gray Al_3Ni particles are readily visible.

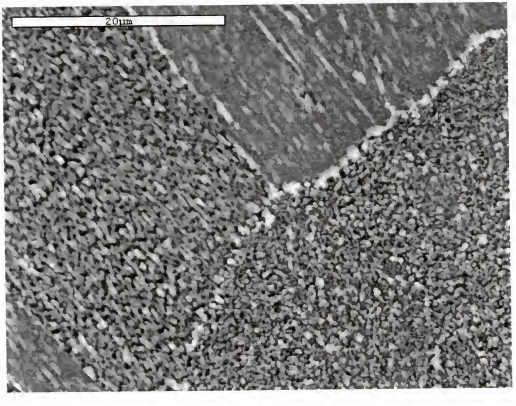

Figure 4.8 BSE image of eutectic microstructure showing accelerated coarsening of intermetallics at eutectic grain boundaries.

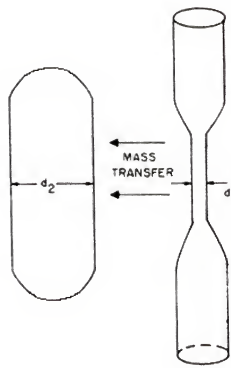

Figure 4.9 Schematic of fragmentation of rod shaped phases in initial stage of Ostwald ripening, where d_1 decreased as d_2 increases.[73]

CHAPTER 5
MICROSTRUCTURES AND CRYSTALLOGRAPHY OF THE DIRECTIONALLY SOLIDIFIED ALUMINUM-CERIUM-NICKEL TERNARY EUTECTIC SYSTEM

Background

Microstructures are the critical link between processing and materials properties, and are key in the development of alloy systems. Directional solidification (DS) is a processing route that, due to the unique microstructures which result, has been widely employed in the investigation and production of many structural alloys. The distinctive characteristic of directional solidification is the particularly potent means of controlling the heat flow of the casting process, via application of thermal gradients across the liquid/solid interface and appropriate growth velocities. Such solidification conditions can result in microstructures comprised of an oriented phase, or alignment of multiple phases, in the direction of solidification which can result in favorable microstructures and properties.

One of the most significant advancements made via DS processing is that of the development of single crystal structural alloys, as well as alloys comprised of microstructures with oriented strengthening phases in the proposed direction of loading for elevated temperature service. The technology of single crystal alloys was pioneered by Pratt and Whitney Aircraft in the mid 1960's, but was not widely employed until the mid 1970's when the single crystal alloy PWA 1480

was shown to offer superior properties in comparison to the columnar grain DS MAR-M 200 alloy.[30]

In addition to the development of single crystal alloys for high temperature service in turbine engine applications, investigations of DS eutectics for elevated temperature service have also been pursued.[30] Much of this work was initiated in the late 1960's when Kraft proposed and studied the application of the same DS technology employed to process the current superalloys could be applied to form in-situ composites if performed on alloys which form multiple phases on solidification, such as eutectics.[99] Kraft's work was also pursued by other researchers, such as Tewari, who investigated the DS of several iron-based eutectics.[100] Specifically, Tewari developed eutectic microstructures from the DS of Fe-25Ta-22Ni-10Cr and Fe-15.5Nb-14.5Ni-6Cr pseudo-binary eutectics.[100] These eutectic microstructures, generated at high thermal gradients and low velocities (i.e., 0.5 cm/hour), consisted of an α-iron matrix with oriented intermetallics of Fe_2Ta for the Fe-25Ta-22Ni-10Cr alloy and Fe_2Nb for the Fe-15.5Nb-14.5Ni-6Cr alloy, with the Ni added as a FCC matrix stablizer and the Cr as a solid solution strengthener.[95,100] These DS eutectics had favorable strength parallel to the growth direction and high microstructural stability under thermal cycling, but proved to be too difficult to cast for extensive commercial application due to the high thermal gradients and low growth velocity required.[100,101]

Investigators have performed similar DS studies to those performed by Tewari on a wide array of eutectics, and have made considerable advances in the control of microstructures as well as the resulting strength properties, with the

vast majority of work performed on either binary or pseudo-binary compositions.[49,77,88,93,101-105] Due to their complexity, only recently has the solidification of ternary eutectics been more thoroughly investigated.[51,52] In recent work by Belov and Naumova, the Al-Ce-Ni ternary eutectic was discovered, with the eutectic microstructure found to be comprised of aluminum-nickel and aluminum-cerium intermetallics, whose combined volume fraction was approximately 0.25.[1] Belov and Naumova also speculated that the Al-Ce-Ni, as well as some other similar ternary systems, could be potential candidates for further studies for strong, light-weight applications if a fine uniform distribution of the two intermetallics within the microstructure could be obtained.[1] It was also suggested that the Al-Ce-Ni structures, since comprised of equilibrium phases formed from the melt on solidification, would perform superior in elevated temperature applications in comparison with other aluminum-based precipitation hardened, ODS, or RSP alloys.[1] Thus, in addition to the lack in the understanding of the solidification of the microstructures in ternary eutectic systems, the investigation of the Al-Ce-Ni system also offers an opportunity to explore it as a possible alloy for use in strong light-weight, elevated temperature applications. To address this current lack of knowledge of the evolution of ternary microstructures and the possible future application of the Al-Ce-Ni ternary eutectic, the present study was focused on the directional solidification of the Al-12 wt% Ce-5 wt% Ni ternary eutectic.

Experimental Work

Buttons of the Al-12 wt% Ce-5 wt% Ni ternary and Al- 4.7 wt% Ni binary eutectic compositions were prepared from high purity elements in a non-

consumable arc melting furnace as described in previous chapters. The eutectic buttons were sectioned and placed in tubular alumina crucibles 15mm diameter and 6.5 cm tall. Directional solidification was performed in a Centorr high temperature DS furnace (Figure 5.1). The chamber was evacuated to 10^{-2} Torr and flushed with argon to –50 kPa. This cycle was repeated three times in succession to promote an oxygen depleted atmosphere. Ti sponge material was also placed in the vacuum furnace chamber to promote an oxygen depleted atmosphere throughout the DS process. The ternary eutectic composition was remelted at 680°C, held for 30 minutes, and directionally solidified at a velocity of 17 mm/min. Similarly, the DS of the binary Al-Ni eutectic was performed by remelting at 680°C, hold for 30 minutes, and then withdrawn from the chamber at 17 mm/min.

Longitudinal and transverse samples were sectioned from the DS ingots, which were then polished through 0.3 μm alumina for optical and scanning electron microscopy. TEM analysis was performed on both longitudinal and transverse sections. Samples for TEM analysis were prepared by initial thinning with SiC paper followed by jet polishing in a 1 part perchloric acid, 2 part ethylene glycol, 7 part methanol solution at –25°C , 30 mA, and 12 mV.

SEM analysis was performed on either a JEOL 6400 or a 6315F scanning electron microscope, both equipped with energy dispersive spectrometers (EDS) and accompanying Oxford microanalysis hardware with Link ISIS software for compositional analysis. TEM analysis was performed on a Philips EM 420 with an EDAX detector and accompanying data analysis software.

Results

Microstructures of the DS ternary composition were fully eutectic and were comprised of the orthorhombic $Al_{11}Ce_3$ (a = 0.439 nm, b = 1.302 nm, c = 1.009nm), and orthorhombic Al_3Ni (a = 0.661 nm, b = 0.737 nm, c = 0.481 nm) intermetallics, in an aluminum matrix (a_o = 0.405 nm). Characteristic SADP for each of the cube directions of the intermetallics are shown in Appendix A. Figures 5.2 and 5.3 illustrate characteristic BSE images of longitudinal and transverse sections. Similar to observations of the microstructures of wedge-cast ingots discussed earlier, the ternary DS microstructures consist of chain-like structures comprised of alternating $Al_{11}Ce_3$ and Al_3Ni intermetallics. The ternary microstructures show the majority of the $Al_{11}Ce_3$ phases formed as rods, and with the remainder forming as plates (Figure 5.4a). Alternatively, the Al_3Ni intermetallics form as either rods or spheres (Figure 5.4b), with the long axis of both of the intermetallics extending parallel to the growth direction.

The characteristic <100>αAl was found to be parallel to the growth axis in all of the samples taken from sections transverse to the growth direction for TEM analysis of the microstructures. Surprisingly, no directions in either of the $Al_{11}Ce_3$ or Al_3Ni phases were exactly parallel to the growth direction. However, the [100]$Al_{11}Ce_3$ was observed ~2° from the growth direction, and the [130]Al_3Ni ~5° from the growth direction.

Continued TEM analysis, however, revealed the following orientation relationship: the <1$\underline{1}$0>αAl // [3$\underline{1}$0]$Al_{11}Ce_3$, {001}αAl // (001)$Al_{11}Ce_3$ (Figure 5.5), and <100>αAl // [001]Al_3Ni, {1$\underline{1}$0}αAl // (210)Al_3Ni (Figure 5.6), which is

consistent with the previous observations. Faceting of the Al_3Ni and $Al_{11}Ce_3$ intermetallics was also observed (Figure 5.7). As illustrated in Figure 5.7a, the largest Al_3Ni facets were observed to form parallel to (101) and smaller facets on (100). Alternatively, as shown in Figure 5.7b, the majority of the facets of the $Al_{11}Ce_3$ intermetallics were observed to form on (010).

The microstructures of the Al-Ni binary DS ingot were also fully eutectic. Characteristic BSE and TEM images of longitudinal and transverse sections are illustrated in Figures 5.8 and 5.9, respectively. TEM revealed a <001>αAl // [104]Al_3Ni, {100}αAl // (401)Al_3Ni orientation relationship for the Al-Ni binary eutectic (Figure 5.10).

Discussion

The microstructures formed on solidification of the Al-Ce-Ni ternary eutectic are comprised of two faceting phases ($Al_{11}Ce_3$ and Al_3Ni) in a non-faceting aluminum matrix. Within the ternary eutectic composition, the calculated equilibrium volume fraction of the intermetallic phase is 0.316 and 0.117 for the $Al_{11}Ce_3$ and Al_3Ni, respectively. (Appendix B). Jackson and Hunt have shown the tendency for the minor phase in a binary eutectic to form as rods upon solidification if it's volume fraction falls below $1/\pi$, and as plates if the volume fraction of the minor phase in the eutectic is above this value.[49] Similarly, Kurz and Fisher, have also published results concerning a lamellar to rod transition in the morphology of the minor phase of the eutectic systems.[60] However, their studies have shown that this lower limit of volume fraction for plate formation occurs at 0.28.[60] Jackson and Hunt also proposed that the formation of the minor

phase as rods minimizes the surface area per unit volume while maintaining conditions which allow efficient diffusion of solutes in the liquid during solidification.[49] Following this proposal, the plate, rod, or spherical morphology of the minor phase in binary non-faceted/non-faceted eutectics can also be predicted by estimating the surface area per volume for each of the shapes (Appendix C). These calculations can also be expressed graphically to illustrate the morphology, which forms on solidification in order to minimize surface area per unit volume as a function of volume fraction (Figure 5.11). If, for any given volume fraction, the favored morphology of the minor phase is that which possess the least surface area per unit volume, these calculations suggest that, in addition to the lower limit in the volume fraction in which plates form on solidification at $1/\pi$, spheres, instead of rods, of the minor phase are likely to form if the volume fraction of the minor phase in the binary eutectic drops below ~0.15.

Prior observations of the relationship between the volume fraction of the minor phase in the eutectic and its morphology, as well as the calculations, which predict the morphology, however, consider only non-faceted/non-faceted eutectic systems, and do not consider interfacial energy contributions in the faceted/non-faceted binary systems. One method of addressing such contributions is in examination of the calculations, which predict such morphology in the Appendix. Any consideration of interfacial energy would be added to the surface area term. This would shift the volume fraction at which a transition from plates to rods, or rods to spheres, to slightly higher values. Considering this, in addition to the previous observations made by Kurz as well as Fisher and Jackson and Hunt, it

is not surprising to find the microstructures of the Al-Ce-Ni ternary eutectic comprised of either plates or rods of the $Al_{11}Ce_3$ intermetallics, and rods or spheres of Al_3Ni, as seen in Figures 5.3, and 5.4. The volume fraction of $Al_{11}Ce_3$ in the ternary eutectic has been calculated to be 0.316. This value is slightly greater than the proposed value $1/\pi$ or 0.28, below which rods of the minor phase will form and above which plates will form.[49,60] Similarly, the volume fraction of Al_3Ni in the ternary eutectic is 0.117, which is also very close to the calculated value for the lower limit of rod formation, 0.15, below which spheres are predicted to solidify. Nether of the $Al_{11}Ce_3$ or Al_3Ni volume fractions in the eutectic are substantially different than that of the calculated or previously published values in which a plate to rods or rods to sphere transition occurs, thus allowing plates and rods of $Al_{11}Ce_3$ to form as well as rods and spheres of Al_3Ni.

The observed orientation relationship between the matrix and each of the intermetallics, $<1\bar{1}0>\alpha$ Al // $[3\bar{1}0]Al_{11}Ce_3$, $\{001\}\alpha$Al // $(001)Al_{11}Ce_3$ and $<100>\alpha$ Al // $[001]Al_3Ni$, $\{\bar{1}10\}\alpha$Al // $(210)Al_3Ni$, implies the following orientation relationship between the $Al_{11}Ce_3$ and Al_3Ni phases: $[001]Al_{11}Ce_3$ // $[001]Al_3Ni$, $(210)Al_{11}Ce_3$ // $(\bar{1}30)Al_3Ni$. This is consistent with TEM results and is depicted in the stereographic projections in Figures 5.12-14 for the ternary eutectic. In further examination of the orientation relationship between the α-Al matrix and the $Al_{11}Ce_3$ phase, due to the symmetry of the orthorhombic $Al_{11}Ce_3$ intermetallic, the following planes are also parallel: $\{110\}\alpha$Al // $(130)Al_{11}Ce_3$ (Figure 5.5). Comparison of the interplanar spacing between $\{110\}\alpha$Al // $(130)Al_{11}Ce_3$, reveals a 7% difference. Though the growth direction of the $Al_{11}Ce_3$ is offset ~2° from

that of that of the α-Al the 7% difference in interplanar spacing between the two phases may contribute to the observed orientation relationship. Alternatively, there are no directions in the Al_3Ni phase which are found parallel to the growth direction, nor is there a similarity between the interplanar spacing of the $\{1\bar{1}0\}\alpha Al$ and the $(210)Al_3Ni$ which are parallel. However, the difference in interplanar spacing between the parallel planes of the $Al_{11}Ce_3$ and Al_3Ni phases is minimal, i.e., there is only 0.3% difference between the interplanar spacing of the parallel $(210)Al_{11}Ce_3$ and $(1\bar{3}0)Al_3Ni$, which may result in the observed orientation relationship.

The Al-Ni binary eutectic was also studied in an attempt to bring further insight of the microstructural evolution of the Al-Ce-Ni ternary eutectic. The Al/Al_3Ni orientation relationship for the binary Al-Ni system was observed to differ from that determined for the ternary eutectic system. In the case of the Al-Ni binary eutectic, the orientation relationship is $<001>\alpha Al$ // $[104]Al_3Ni$, $\{100\}>\alpha Al$ // $(401)Al_3Ni$. This orientation relationship also implies that the {202}Al is also parallel to $(203)Al_3Ni$. The difference in interplanar spacing between these planes is 0.6%, which may result in the observed orientation relationship of the binary Al-Ni eutectic. The orientation relationship of the Al-Ni binary eutectic, $<001>\alpha Al$ // $[104]Al_3Ni$, $\{100\}>\alpha Al$ // $(401)Al_3Ni$, however, is different that that of the Al-Ce-Ni ternary eutectic, $<100>\alpha Al$ // $[001]Al_3Ni$, $\{1\bar{1}0\}\alpha Al$ // $(210)Al_3Ni$. This suggests that the Al_3Ni may nucleate with an orientation relationship governed by the $Al_{11}Ce_3$ intermetallic with which it shares an interface.

In order to discuss the unique formation of the chain-like structures of alternating $Al_{11}Ce_3$ and Al_3Ni intermetallics in the Al-Ce-Ni ternary eutectic, the diffusion of solutes during solidification must be considered. In the case of binary eutectics, it is well understood that upon solidification, each of the two solidifying phases must reject solute into the liquid ahead of the advancing solidification front.[49,60] Solute rejected from one of the phases in needed by the other.[49,60] Thus in eutectics with a volume fraction of the minor phase greater than $1/\pi$, the lamellar structure is favored, providing a lateral path for diffusion of the solutes on solidification and minimizing solute buildup for both phases at the solid/liquid interface.[60]

Additionally, in the case of the non-faceted/faceted binary eutectics presented by Verhoeven (Figure 5.15), the non-faceted phase leads the solidification front while rejecting solute into the adjacent liquid, while the faceted phases, with a higher entropy of fusion, will be undercooled slightly then form immediately behind the non-faceted phase.[37] In the case of the ternary eutectic, the aluminum phase should lead the solidification front, rejecting cerium and nickel into the liquid at the solid/liquid interface, and the $Al_{11}Ce_3$ and Al_3Ni phases should form immediately behind the aluminum, and likewise reject the corresponding solute into the liquid at the solid/liquid interface. Assuming each of the aluminum, $Al_{11}Ce_3$, and Al_3Ni phases reject a component which is required by one of the other phases on solidification, they must solidify in close proximity, or share an interface, to promote the most efficient path for diffusion (Figure 5.16).

This is consistent with the unique alternating $Al_{11}Ce_3/Al_3Ni$ phases observed in the ternary eutectic (Figures 5.3, and 5.4).

These observations, however, also imply that it may not be possible to form a homogeneous distribution of multiple independent phases throughout a continuous matrix on solidification. As in the case of the ternary Al-Ce-Ni eutectic, the solidification of the $Al_{11}Ce_3$ and Al_3Ni intermetallic phases from the melt results in a microstructure in which the two Al-rich phases share a common interface. This is likely to be the case in other systems. Thus it may not be possible to generate structures comprised of multiple product phases in a continuous matrix formed from a single parent phase on solidification. Such transformations require solute diffusion, and the formation of structures similar to those observed in the Al-Ce-Ni ternary eutectic, comprised of multiple phases which share a common interface, would occur allowing an efficient pathway for diffusion and minimize surface area per unit volume of the phases within the matrix.

Conclusions

The Al-12wt% Ce-5wt% Ni ternary eutectic was cast via directional solidification. Fully eutectic microstructures produced via DS resulted in a unique microstructure comprised of a chain-like array of alternating $Al_{11}Ce_3$-Al_3Ni intermetallics. The intermetallics in the ternary eutectic were found to exhibit $<1\bar{1}0>\alpha Al$ // $[3\bar{1}0]Al_{11}Ce_3$, $\{001\}\alpha Al$ // $(001)Al_{11}Ce_3$, and $<100>\alpha Al$ // $[001]Al_3Ni$, $\{1\bar{1}0\}\alpha Al$ // $(210)Al_3Ni$ orientation relationships. Faceting of both the Al_3Ni and $Al_{11}Ce_3$ phases was observed, with the largest Al_3Ni facets forming on (101) and

smaller facets on (100), and the majority of the facets of the $Al_{11}Ce_3$ intermetallics were forming on (010). It is proposed that the unique microstructure and the resultant orientation relationships observed are driven by the solute diffusion profile at the solid/liquid interface during solidification. This suggests that, for ternary eutectic systems such as that of this study as well as other systems which involve the liquid→solid transformations of a single parent phase to multiple product phases, it may not be possible to form a microstructure comprised of a homogeneous distribution of two or more product phases.

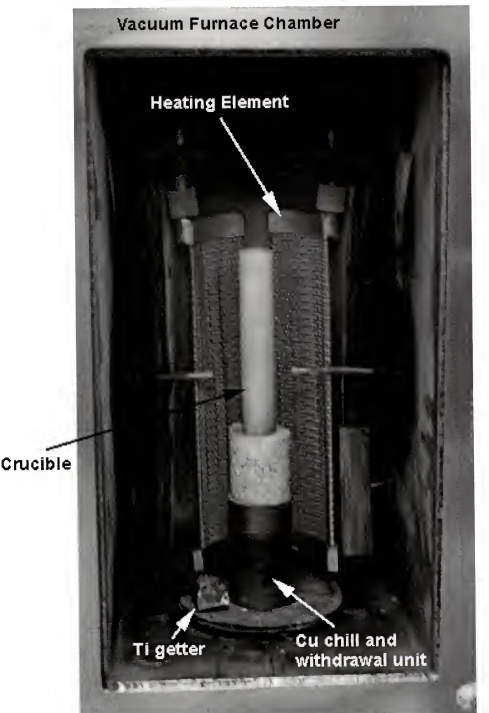

Figure 5.1 Centorr high temperature vacuum withdrawal chamber used for the directional solidification studies.

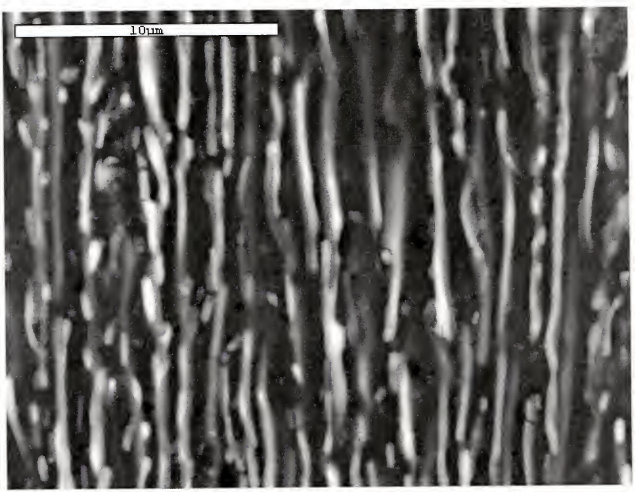

Figure 5.2 BSE image of longitudinal section of ternary eutectic Al-12Ce-5Ni DS ingot with $Al_{11}Ce_3$ intermetallics (white) and Al_3Ni intermetallics (gray).

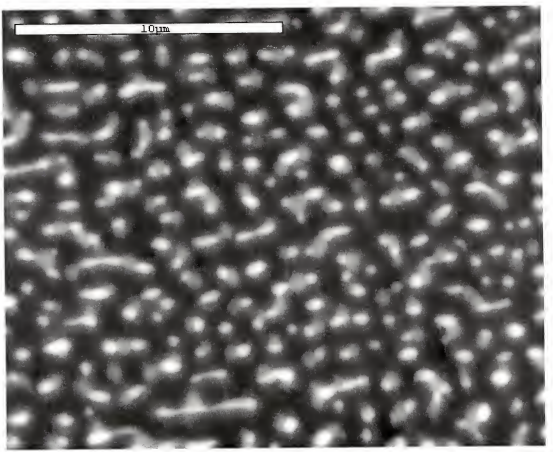

Figure 5.3 BSE image of transverse section of ternary eutectic Al-12Ce-5Ni DS ingot with unique microstructure consisting of $Al_{11}Ce_3$ intermetallics (white) and Al_3Ni intermetallics (gray).

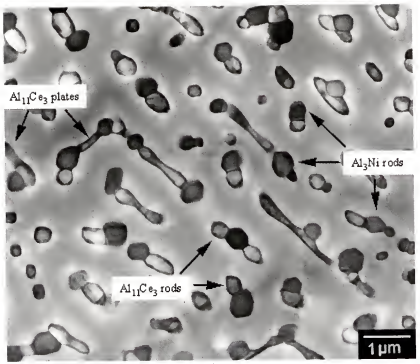

a)

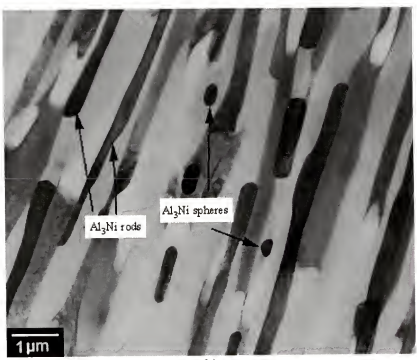

b)

Figure 5.4 BF TEM image of a) transverse section illustrating $Al_{11}Ce_3$ plates and rods and b) longitudinal section illustrating Al_3Ni rods and spheres (highly diffracting dark gray intermetallics are Al_3Ni and the light gray are $Al_{11}Ce_3$)

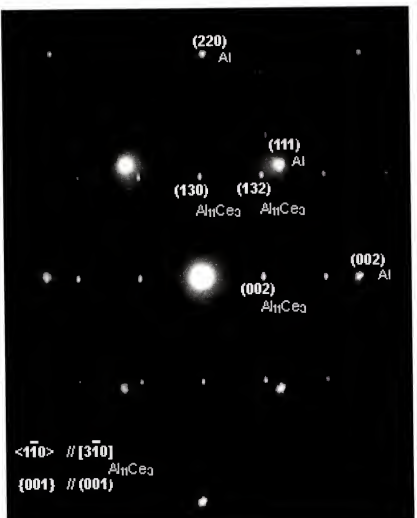

Figure 5.5 SADP from $Al_{11}Ce_3$ and α-Al matrix illustrating <110>αAl // [3$\bar{1}$0]$Al_{11}Ce_3$, {001}αAl // (001)$Al_{11}Ce_3$, orientation relationship.

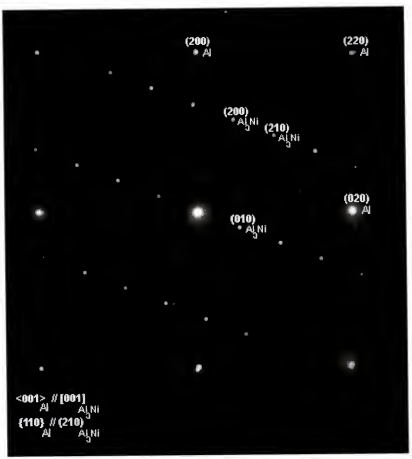

Figure 5.6 SADP from Al_3Ni intermetallic and α-Al matrix illustrating <001>αAl // [001]Al_3Ni, {110}αAl // (210)Al_3Ni orientation relationship.

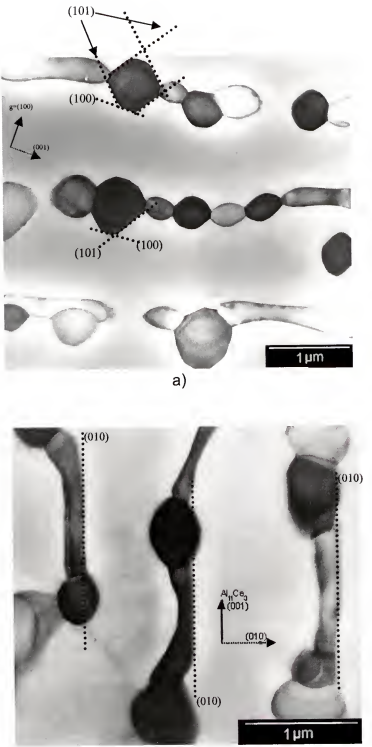

Figure 5.7 BF TEM image of a) alternating $Al_{11}Ce_3$-Al_3Ni particles illustrating planes of which facet form on the intermetallics (highly diffracting dark gray intermetallics are Al_3Ni and the light gray are $Al_{11}Ce_3$) and b) BF TEM image of faceting planes of $Al_{11}Ce_3$.

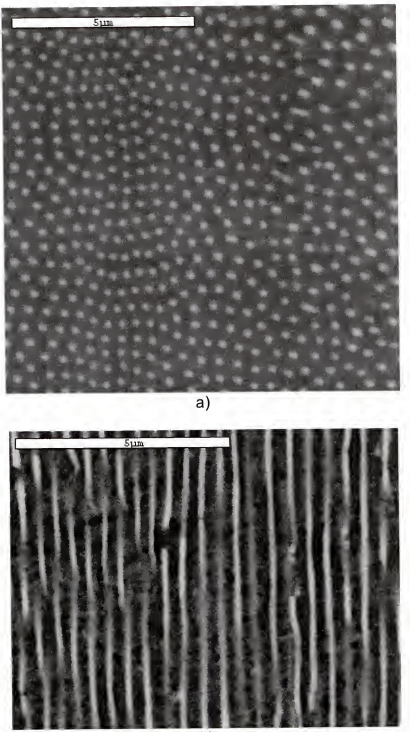

Figure 5.8 BSE image of a) transverse section of DS Al-5Ni binary eutectic Ingot, b) BSE of longitudinal section from same ingot.

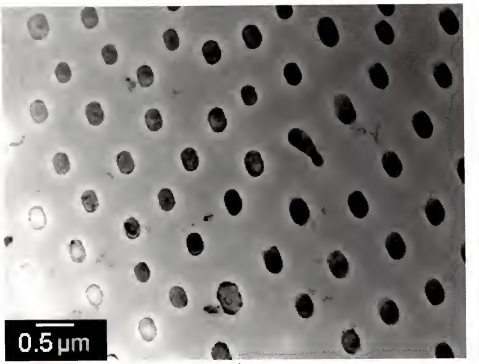

a)

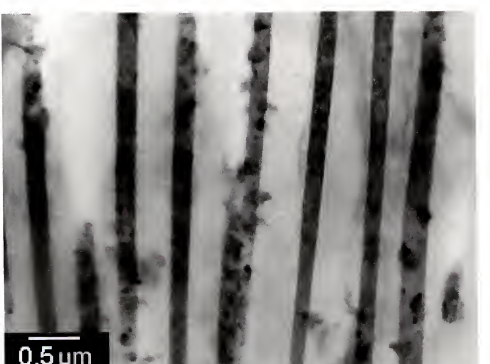

b)

Figure 5.9 BF TEM image of a) transverse section of DS Al-5Ni binary eutectic Ingot, b) BSE of longitudinal section from same ingot. The mottling in b) is due to contamination of the TEM foil.

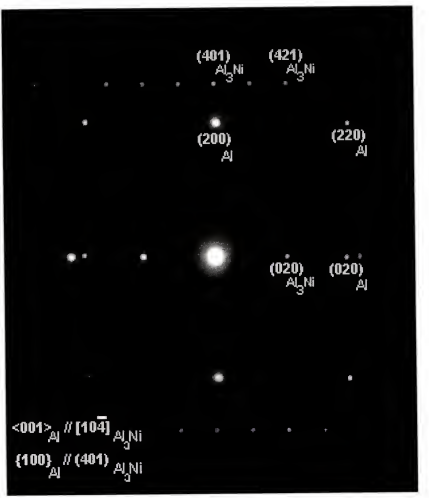

Figure 5.10 SADP from Al_3Ni intermetallic in α-Al matrix of Al-Ni binary eutectic illustrating <001>αAl // [10$\bar{4}$]Al_3Ni, (100)αAl // (401)Al_3Ni orientation relationship. The growth direction is out of the page.

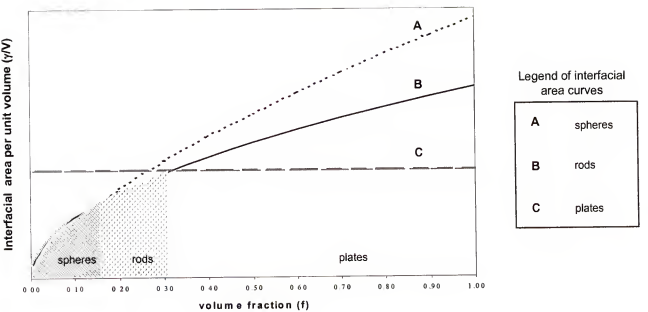

Figure 5.11 Interfacial area per unit volume as a function of volume fraction for plates, rods, and spheres of the minor phase in binary eutectics. For any given volume fraction, in order to minimize the interfacial area per unit volume, the morphology of the minor phase is predicted to form as spheres at volume fractions below 0.15, as rods when the volume fraction is between 0.15 and $1/\pi$, and as plates when the volume fraction of the minor phase in the system is greater than $1/\pi$.

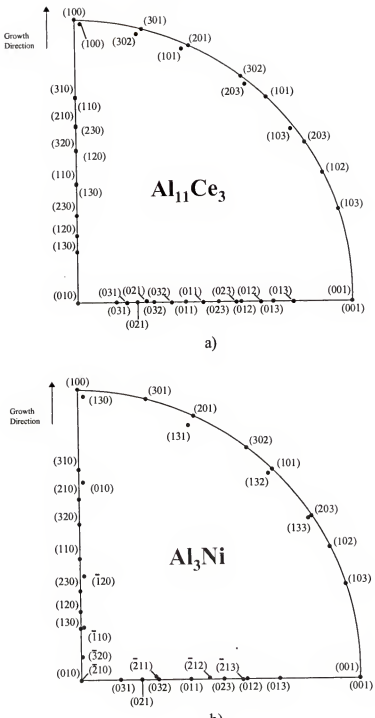

Figure 5.12 Stereographic projections of a) (hkl) $Al_{11}Ce_3$ superimposed on (hkl)α-Al and, b) (hkl) Al_3Ni superimposed on (hkl) α-Al, and of intermetallic for the ternary eutectic microstructure. The center of the poles is indicated in the lower left corner of each of the projections, with the α-Al planes labeled outside of the quadrant and the intermetallic labels inside.

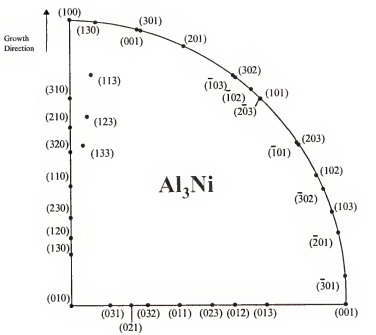

Figure 5.13 Stereographic projection of (hkl) Al_3Ni superimposed on (hkl) α-Al for the DS Al-Ni binary eutectic. The center of the poles is indicated in the lower left corner of each of the projections, with the α-Al planes labeled outside of the quadrant and the intermetallic labels inside.

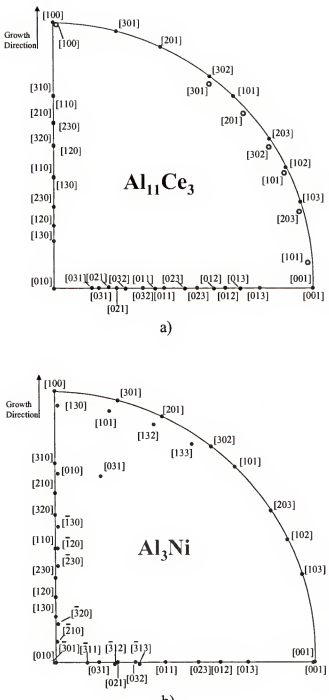

Figure 5.14 Stereographic projections of a) [uvw] $Al_{11}Ce_3$ superimposed on [uvw]α-Al and, b) [uvw] Al_3Ni superimposed on [uvw] α-Al, and of intermetallic for the ternary eutectic microstructure. The center of the poles is indicated in the lower left corner of each of the projections, with the α-Al planes labeled outside of the quadrant and the intermetallic labels inside.(Note: Open circles represent directions behind quadrant.).

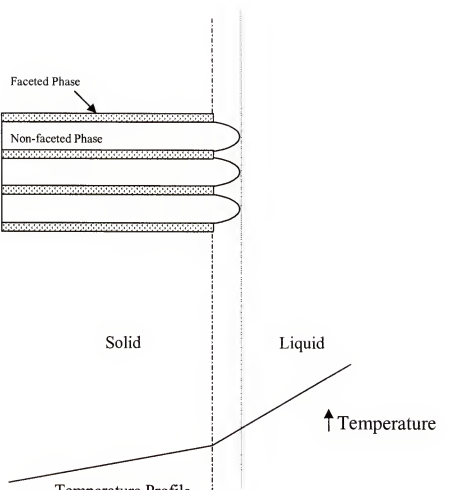

Figure 5.15 Profile of intermetallic phases in a faceted/non-faceted eutectic system growing into a positive thermal gradient.[37]

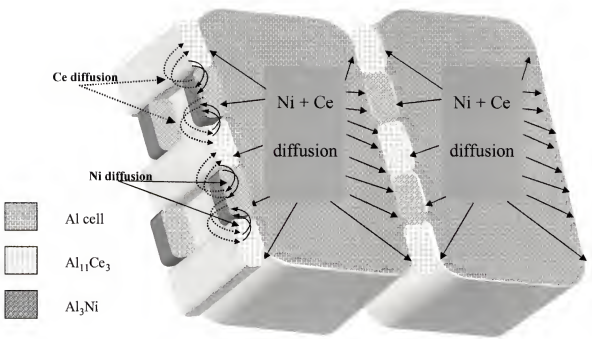

Figure 5.16 Schematic of diffusion profile for growth of Al-Ce-Ni ternary eutectic at the solid/liquid interface. The solid, straight arrows indicate the diffusion of both Ce and Ni as the Al leads the solidification front. At the chain of alternating $Al_{11}Ce_3/Al_3Ni$ intermetallics, the curved arrows depict the diffusion of Ce and Ni as each of the neighboring phases rejects solute which is required for growth by the other.

CHAPTER 6
CONCLUSIONS

The solidification, microstructural selection, stability of the microstructures, and crystallography of the Al-Ce-Ni ternary eutectic were characterized. The results indicate:

The cooperative growth regime for the Al-Ce-Ni ternary system is similar to that of a binary faceted/non-faceted system. The ternary eutectic cooperative growth regime is skewed towards higher concentrations of Ce and Ni; thus, the ternary eutectic microstructure can be solidified from the melt at hypereutectic compositions with sufficient growth velocity. The Al_3Ni phase, however, is weakly faceted in comparison to the $Al_{11}Ce_3$, and forms at a faster rate than on solidification. However, though the Al_3Ni phase forms at a faster rate, it's volume fraction is considerably lower than that of $Al_{11}Ce_3$, causing the spheres or rods of Al_3Ni to nucleate on the more continuous plates or rods of $Al_{11}Ce_3$. The α-Al + $Al_{11}Ce_3$ + Al_3Ni eutectic system is a non-faceted/weakly-faceted/faceted ternary system with a microstructure comprised of a unique array of chain-like structures of alternating $Al_{11}Ce_3$ and Al_3Ni intermetallics.

The intermetallics formed on solidification of the Al-12wt% Ce-5wt% Ni eutectic are equilibrium phases, which did not transform to other phases after extended thermal exposures of up to 100 hours at 550°C. The as-cast microstructure, however, coarsens from its original fine structure at exposures of over an hour at 400°C. With prolonged exposure at 400°C or greater, coarsening

of the chain-like microstructure of alternating $Al_{11}Ce_3/Al_3Ni/Al_{11}Ce_3$ intermetallics occurs via initial fragmentation of the intermetallics followed by further coarsening via a classic Ostwald ripening mechanism. Accompanying the coarsening of the microstructure, a decrease in the hardness occurs. The coarsening of the microstructure occurs via multiple mechanisms: a) classic Ostwald ripening of the intermetallics within the eutectic grains, as mentioned previously, and b) an accelerated coarsening at the grain boundaries due to the increased diffusion at the boundaries

The fully eutectic microstructure of the DS Al-12wt% Ce-5wt% Ni ternary eutectic is comprised of a unique chain-like array of alternating $Al_{11}Ce_3$-Al_3Ni-$Al_{11}Ce_3$ intermetallics. The intermetallics in the ternary eutectic exhibit $<\bar{1}10>\alpha Al$ // $[\bar{3}10]Al_{11}Ce_3$, $\{001\}\alpha Al$ // $(001)Al_{11}Ce_3$, and $<100>\alpha Al$ // $[001]Al_3Ni$, $\{\bar{1}10\}\alpha Al$ // $(210)Al_3Ni$ orientation relationships. Faceting of the Al_3Ni and $Al_{11}Ce_3$ occurs with the largest Al_3Ni facets forming on (101) and smaller facets on (100). Alternatively, the majority of the facets of the $Al_{11}Ce_3$ intermetallics form on (010). The unique microstructures are driven by the solute diffusion profile at the solid/liquid interface during solidification. This suggests that on the solidification of ternary eutectic systems in general, it may not be possible to form a microstructure which consists of the two minority product phases which does not share a common interface. Furthermore, this also implies that it may not possible to generate a microstructure comprised of a homogeneous distribution of multiple product phases in a continuous matrix on solidification from a single parent phase.

APPENDIX A
SELECTED AREA DIFFRACTION PATTERNS

Characteristic selected area diffraction patterns (SADP) from the cube directions of $Al_{11}Ce_3$:

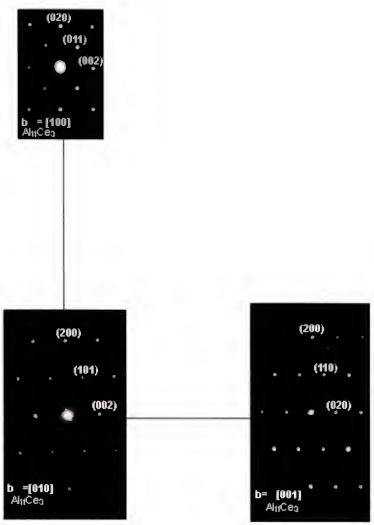

Characteristic SADP from the cube directions of Al_3Ni:

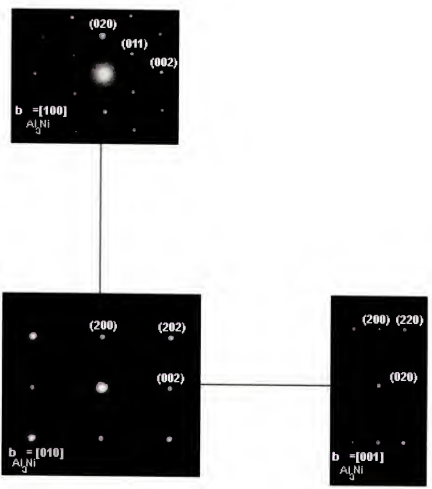

APPENDIX B
VOLUME FRACTION OF PHASES IN TERNARY EUTECTIC

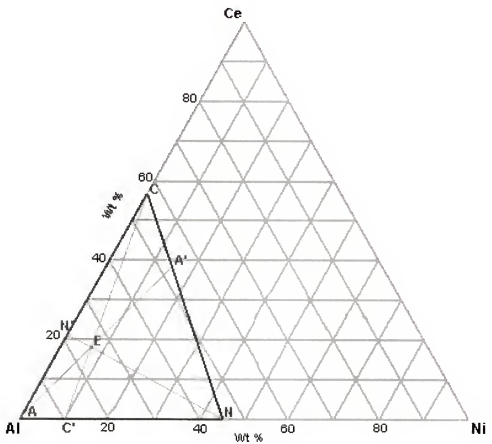

Considering negligible solubility of Ce or Ni in α-Al, and no solubility of Ce in Ni or Ni in Ce, the volume fractions of each of the $Al_{11}Ce_3$ and Al_3Ni phases in the ternary eutectic can be predicted from the tie-triangles drawn in the 3-phase field.

$$\text{Volume fraction of } Al_{11}Ce_3 = \frac{C'E}{C'C} = 0.316$$

$$\text{Volume fraction of } Al_3Ni = \frac{N'E}{N'N} = 0.117$$

APPENDIX C
SURFACE AREA PER VOLUME FOR MINOR PHASES

The following equations and derivation express the transition in the morphology of the minor phase in a non-faceted/non-faceted eutectic system in terms of interfacial area per volume of solid and volume fraction, and assumes microstructure will form lowest energy.

Plate Formation

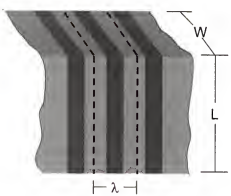

$$\text{Surface area (S.A.)}_{\text{Plate}} = L * W * 2 \qquad (1)$$

$$\text{Interfacial area per unit volume } (\gamma)_{\text{Plate}} = \frac{L * \text{W} * 2}{\lambda}$$

(where $\lambda = d$ and $L = W = 1$)

$$\gamma_{\text{Plate}} = \frac{2}{d} \qquad (2)$$

Which is independent of volume fraction

Rod Formation

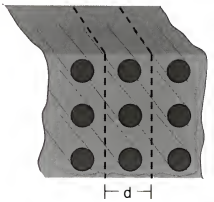

$$\text{S.A.}_{\text{Rods}} = \frac{2 * \pi * r * L}{d} \qquad (3)$$

$$\text{where } \frac{1}{d} = \text{number of rods/unit length}$$

$$\gamma_{\text{Rods}} = \frac{2 * \pi * \text{r}}{d^3} \qquad (4)$$

$$\text{Volume fraction of minor phase in eutectic } (f)_{\text{Rods}} = \frac{\pi * r * L}{d^2} \qquad (5)$$

Solving the equations for interfacial area per unit volume (4), and volume fraction of the minor phase of the eutectic (5) simultaneously yields the following equation (6), which describes interfacial area per unit volume as a function of volume fraction of minor phase in eutectic:

$$\gamma_{\text{Rods}}(f) = \frac{2}{d} * \sqrt{f\pi} \qquad (6)$$

Solving the interfacial area per unit volume as a function of volume fraction equations $\gamma(f)$ for both plate (2) and rod (6) formation yields the volume fraction upon which the rod to plate transition of the minor phase of the eutectic occurs as volume fraction is increased:

$$\frac{2}{d} = \frac{2}{d} * \sqrt{f\pi} \qquad (7)$$

$$f = \frac{1}{\pi}$$

Therefore, the transition from plates to rods should occur at approximately $1/\pi$.

Sphere formation

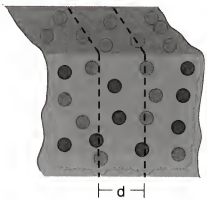

$$S.A._{Spheres} = \frac{4 * \pi * r^2}{d} \qquad (8)$$

$$\text{where } \frac{1}{d} = \text{number of spheres/unit length}$$

$$\gamma_{Spheres} = \frac{4 * \pi * r^2}{d^2} \qquad (9)$$

$$\text{Volume fraction of minor phase in eutectic } (f)_{Spheres} = \frac{\left(\frac{4}{3}\right)\pi * r^3}{d^2} \qquad (10)$$

Solving the equations for interfacial area per unit volume (9), and volume fraction of the minor phase of the eutectic (10) simultaneously yields the following equation (11), which describes the interfacial area per unit volume as a function of volume fraction of the minor phase in eutectic:

$$\gamma_{Spheres}(f) = \left(\frac{4 * \pi}{d^2}\right) * \left(\frac{3 * f * d^2}{4 * \pi}\right)^{2/3} \qquad (11)$$

Solving the interfacial area per unit volume as a function of volume fraction equations $\gamma(f)$ for both plate (6) and rod (11) formation ,or graphing both equations, yields the volume fraction upon which the sphere to rod transition occurs, as volume fraction is increased; which is determined to occur at ~0.15 (Figure 5.11). Thus the transition from spherical particles to rods of the minor phase in the eutectic system should occur at a volume fraction of ~0.15.

BIBLIOGRAPHY

1. Belov, N. A. and Naumova, E. S. Prospects for the Design of Structural Cast Eutectic Al-Ce-Ni Alloys. Russian Metallurgy. 1996; (6): p. 130-136.

2. King, F. Aluminum and Its Alloys. Ellis Horwood Limited: Chichester, 1987.

3. Harding, A. R. Aluminum Alloys for Structural Applications. *In*: Aluminum Transformation Technology and Applications, Pampillo, C. A., Biloni, H., and Embury, D. E., Editors. American Society for Metals: Metals Park, Ohio, 1978.

4. Quist, W. E. and Lewis, R. E. The Need for Rapidly Solidified Powder Metallurgy Aluminum Alloys for Aerospace Applications. *In*: Rapidly Solidified Powder Aluminum Alloys. American Society for Testing Materials: Philadelphia, 1986. p. 7-38.

5. Bray, J. W. Properties and Selection: Nonferrous Alloys and Special-Purpose Materials. *In*: Metals Handbook. Lampman, S. R. and Zorc, T. B., Editors. ASM International: Metals Park, Ohio, 1990. vol. 2. p. 29-61.

6. Wilsdorf, H. G. F. Dispersion Strengthening of Aluminum Alloys. *In*: Dispersion Strengthened Aluminum Alloys, Kim, Y.-W. and Griffith, W. M., Editors. The Minerals, Metals & Materials Society: Warrendale, 1988. p. 3-30.

7. Lee, D. Y. and Zupon, D. E. High Temperature Performance of Dispersion Strengthened P/M Aluminum Alloys. *In*: Dispersion Strengthened Aluminum Alloys, Kim, Y.-W. and Griffith, W. M., Editors. The Minerals, Metals & Materials Society: Warrendale, 1988. p. 265-282.

8. Palmer, I. G., Thomas, M. P., and Marshall, G. J. Development of Thermally Stable Al-Cr-Zr Alloys Using Rapid Solidification Technology. *In*: Dispersion Strengthened Aluminum Alloys, Kim, Y.-W. and Griffith, W. M., Editors. The Minerals, Metals & Materials Society: Warrendale, 1988. p. 217-241.

9. Thursfield, G. and Stowell, M. J. Mechanical Properties of Al-8 Wt% Fe-Based Alloys Prepared by Rapid Quenching from the Liquid State. J Mater Sci. 1974; 9(10): p. 1644-1660.

10. Ruggiero, M. A. and Rutter, J. W. Origin of Microstructure in the 332 K Eutectic of the Bi-In-Sn System. Materials Science and Technology. 1997; 13(1): p. 5-11.

11. Rinaldi, M. D., Sharp, R. M., and Flemings, M. C. Growth of Ternary Composites from the Melt: Part II. Metallurgical Transactions. 1972; 3: p. 3139-3148.

12. Rinaldi, M. D., Sharp, R. M., and Flemings, M. C. Growth of Ternary Composites from the Melt: Part I. Metallurgical Transactions. 1972; 3: p. 3133-3138.

13. Rohatgi, P. K. Colony to Two-Phase Dendrite Transition in Al-Al3Ni Eutectic Structures by Additions of Barium, Cerium, and Cedium to the Melt. Metallurgical and Materials Transactions A-Physical Metallurgy and Materials Science. 1970; 1(4): p. 1041-1043.

14. Hawksworth, A., Rainforth, W. M., and Jones, H. Solidification Microstructure Selection in the Al-Rich Al-La, Al-Ce and Al-Nd Systems. Journal of Crystal Growth. 1999; 197(1-2): p. 286-296.

15. Waldman, J. Use of Rapidly Solidified Aluminum Alloys in Land Vehicles. *In*: Rapidly Solidified Powder Aluminum Alloys. American Society for Testing Materials: Philadelphia, 1986. p. 39-43.

16. Adam, C. M. Structure/Property Relationships and Applications of Rapidly Solidified Aluminum Alloys. *In*: Rapidly Solidified Amorphous and Crystalline Alloys, Kear, B. H., Giessen, B. C., and Cohen, M., Editors. Elsevier: New York, 1982. p. 411-422.

17. Mazzolani, F. M. Aluminum Alloy Structures. Pitman: Marshfield, 1985.

18. Skinner, D. J., Okazaki, K., and Adam, C. M. Physical Metallurgy and Mechanical Properties of Aluminum Alloys Containing Eight to Twelve Weight Percent Iron. *In*: Rapidly Solidified Powder Aluminum Alloys. American Society for Testing Materials: Philadelphia, 1986. p. 211-236.

19. Sakata, F. Hypersonic Cruise Vehicle Wing Structure Evaluation. National Aeronautics and Space Administration: Washington, D.C., 1970. vol. NASA CR 1568.

20. Sakata, F. and Davis, G. W. Evaluation of Structural Design Concepts for an Arrow-Wing Supersonic Cruise Aircraft. National Aeronautics and Space Administration: Washington, D.C., 1977. vol. NASA CR 2667.

21. Carllson, C. H. Preliminary Scramjet Design for Hypersonic Air-breathing Missile Application. National Aeronautics and Space Administration: Washington, D.C., 1983. vol. NASA CR 3742.

22. Palmer, I. G., Lewis, R. E., Crooks, D. D., Starke, E. A., and Crooks, R. E. Prospective on the Development of Aluminum-Lithium Alloys. *In*: Aluminum-Lithium Alloys. Sanders, T. H. and Starke, E. A., Editors. The Metallurgical Society of the American Institute of Mining, Metallurgical, and Petroleum Engineers: Warrendale, 1984. p. 217-241.

23. Burke, E. C. Aerospace Applications for Improved Aluminum Alloys. *In*: Aluminum Transformation Technology and Applications. Pampillo, C. A., Biloni, H., and Embury, D. E., Editors. American Society for Metals: Metals Park, Ohio, 1978.

24. Langenbeck, S. L., Griffith, W. M., Hildeman, G. J., and Simon, J. W. Development of Dispersion-Strengthened Aluminum Alloys. *In*: Rapidly Solidified Powder Aluminum Alloys. American Society for Testing Materials: Philadelphia, 1986. p. 410-422.

25. Hatch, J. E. Aluminum : Properties and Physical Metallurgy. American Society for Metals: Metals Park, Ohio, 1984.

26. Reed-Hill, R. E. Physical Metallurgy Principles. Second, ed. D. Van Nostrand: New York, 1973.

27. Lenel, F. V., Backensto, A. B., and Rose, M. V. Properties of Aluminum Powders and of Extrusions Produced from Them. Transactions of the American Institute of Mining and Metallurgical Engineers. 1957; 209: p. 124-130.

28. Grant, N. J. and Preston, O. Dispersed Hard Particle Strengthening of Metals. Transactions of the American Institute of Mining and Metallurgical Engineers. 1957; 209: p. 349-357.

29. Benjamin, J. S. and Bomford, M. J. Dispersion Strengthened Aluminum Made by Mechanical Alloying. Metallurgical Transactions A-Physical Metallurgy and Materials Science. 1977; 8(8): p. 1301-1305.

30. Gilman, P. S. The Physical Metallurgy of Mechanical-Alloyed, Dispersion-Strengthened Al-Li-Mg and Al-Li-Cu Alloys. *In*: Aluminum-Lithium Alloys II,.Sanders, T. H. and Starke, E. A., Editors. The Metallurgical Society of the American Institute of Mining, Metallurgical, and Petroleum Engineers: Warrendale, 1983. p. 485-506.

31. Donochie, S. J. and Gilman, P. S. The Microstructure and Properties of Al-Mg -Li Alloys Prepared by Mechanical Alloying. *In*: Aluminum-Lithium Alloys II. Sanders, T. H. and Starke, E. A., Editors. The Metallurgical Society of the American Institute of Mining, Metallurgical, and Petroleum Engineers: Warrendale, 1983. p. 507-515.

32. Schelleng, R. D. Inco Mechanically Alloyed Products. *In*: Aluminum-Lithium Alloys Design, Development and Application. Kar, R. J., Agrawal, S. P., and Quist, W. E., Editors. ASM International: Metals Park, 1987. p. 57-62.

33. Sanders, T. H. Al-Li-X Alloys-- an Overview. In: Aluminum-Lithium Alloys. Sanders, T. H. and Starke, E. A., Editors. The Metallurgical Society of the American Institute of Mining, Metallurgical, and Petroleum Engineers: Warrendale, 1980. p. 63-67.

34. Adam, C. M. and Das, S. K. The Design of New Engineering Alloys Using Rapid Solidification Technology. In: Rapid Solidification Processing Principles and Technologies. Mehrabian, R. and Parrish, P. A., Editors. Claitor's Publishing Division: Baton Rouge, 1988. p. 66-81.

35. Adam, C. M. Rapid Solidification Processing Methods. *In*: Mechanical Behavior of Rapidly Solidified Materials. Metallurgical Society: Warrendale, 1985. p. 21-39.

36. Kim, N. J. and Das, S. K. High-Performance Light-Weight Alloys by Rapid Solidification Processing. In: Science and Technology of Rapidly Quenched Alloys. Tenhover, M., Johnson, W. L., and Tanner, L. E., Editors. Materials Research Society: Pittsburgh, 1987.

37. Verhoeven, J. D. Fundamentals of Physical Metallurgy. John Wiley & Sons, Inc: New York, 1975: p. 264-283.

38. Hertzberg, R. W. Deformation and Fracture Mechanics of Engineering Materials. John Wiley & Sons, Inc: New York, 1989.

39. Vigier, G., Ortizmendez, U., Merle, P., Thollet, G., and Fouquet, F. Microstructural Stability of Rapidly Quenched Al-Fe Alloys - Influence of Zirconium. Materials Science and Engineering. 1988; 98(Feb): p. 191-195.

40. Willis, T. C. and Cantor, B. Melt-Spinning a Commercial Aluminum Alloy. *In*: Rapidly Solidified Metastable Materials. Kear, B. H. and Giessen, B. C., Editors. Elsevier Science: New York, 1984. p. 131-138.

41. Finn, J. E. Rapid Solidification Technology for Reduced Consumption of Strategic Materials. Noyes: New York, 1985.

42. Zindel, J. W., Stanley, J. T., Field, R. D., and Fraser, H. L. Rapid Solidification and Subsequent Analysis F Some Hypereutectic Aluminum-Based Alloys. Rapidly Solidified Powder Aluminum Alloys. 1984: p. 187-211.

43. Gremaud, M., Carrard, M., and Kurz, W. The Microstructure of Rapidly Solidified Al-Fe Alloys Subjected to Laser Surface-Treatment. Acta Metallurgica Et Materialia. 1990; 38(12): p. 2587-2599.

44. Skinner, D. J., Bye, R. L., Raybould, D., and Brown, A. M. Dispersion Strengthened Al-Fe-V-Si Alloys. Scripta Metallurgica. 1986; 20(6): p. 867-872.

45. Mitra, S. Elevated-Temperature Mechanical-Properties of a Rapidly Solidified Al-Fe-V-Si Alloy. Scripta Metallurgica Et Materialia. 1992; 27(5): p. 521-526.

46. Okazaki, K. and Skinner, D. J. Al-Fe-Zr Alloys for High-Temperature Applications Produced by Rapid Quenching from the Melt. Scripta Metallurgica. 1984; 18(9): p. 911-916.

47. Klar, E. Powder Metallurgy: Applications, Advantages, and Limitations. American Society for Metals: Metals Park, Ohio, 1983.

48. White, J., Willis, T. C., Hughes, I. R., and Jordan, R. M. Metal Matrix Composites Produced by Spray Deposition. *In*: Dispersion Strengthened Aluminum Alloys. Kim, Y.-W. and Griffith, W. M., Editors. The Minerals, Metals & Materials Society: Warrendale, 1988. p. 693-707.

49. Jackson, K. A. and Hunt, J. D. Lamellar and Rod Eutectic Growth. Transactions of the Metallurgical. Society of AIME. 1966; 236: p. 1129.

50. Magnin, P. and Kurz, W. An Analytical Model of the Irregular Eutectic Growth and Its Application to Fe-C. Acta Metallurgica. 1987; 35(5): p. 1119-1128.

51. Juarez-Hernandez, A. and Jones, H. Growth Temperature Measurements and Solidification Microstructure Selection of Primary Al3Ni and Eutectic in the Alpha Al-Al3Ni System. Scripta Materialia. 1998; 38(5): p. 729-734.

52. Hawksworth, A., Rainforth W. M., and Jones, H. A Novel Microstructure in the Al-La-Ni Ternary Eutectic Alloy. Scripta Materialia. 1998; 39(10): p. 1371-1376.

53. Mccartney, D. G., Hunt, J. D., and Jordan, R. M. The Structures Expected in a Simple Ternary Eutectic System .1. Theory. Metallurgical Transactions A-Physical Metallurgy and Materials Science. 1980; 11(8): p. 1243-1249.

54. Mccartney, D. G., Jordan, R. M., and Hunt, J. D. The Structures Expected in a Simple Ternary Eutectic System .2. The Al-Ag-Cu Ternary-System. Metallurgical Transactions A-Physical Metallurgy and Materials Science. 1980; 11(8): p. 1251-1257.

55. Rohatgi, P. K., Sharma, R. C., and Prabhakar, K. V. Microstructure and Mechanical-Properties of Unidirectionally Solidified Al-Si-Ni Ternary Eutectic. Metallurgical Transactions. 1975; A 6(3): p. 569-575.

56. Ruggiero, M. A. and Rutter, J. W. Formation of Microstructure in the Cd-In-Sn Ternary Eutectic. Materials Science and Technology. 1998; 14(3): p. 177-181.

57. Barclay, R. S., Kerr, H. W., and Niessen, P. Off-Eutectic Composite Solidification and Properties in Al-Ni and Al-Co Alloys. Journal of Materials Science. 1971; 6(9x): p. 1168-1184.

58. Wu, Y., Liu, H., and Lavernia, E. J. Solidification Behavior of Al-Si/Sic Mmcs, During Wedge-Mold Casting. Acta Metallurgica Et Materialia. 1994; 42(3): p. 825-837.

59. Ruggiero, M. A. and Rutter, J. W. Microstructure of Bi-Cd-Pb Ternary Eutectic. Materials Science and Technology. 1996; 12(1): p. 7-11.

60. Kurz, W. and Fisher, D. J. Fundamentals of Solidification. Trans Tech: Aedermannsdorf, 1989.

61. Kamio, A. T., H.; Kumai, S.; Takahashi, T. Formation Manner of Monotectic Solidification Structure in Al-in Alloys Solidified Unidirectionally. Journal of the Japan Institute of Metals. 1984; 48(1): p. 84-90.

62. Taylor, J. A., Schaffer, G. B., and Stjohn, D. H. The Role of Iron in the Formation of Porosity in Al-Si-Cu-Based Casting Alloys: Part III. A Microstructural Model. Metallurgical and Materials Transactions A-Physical Metallurgy and Materials Science. 1999; 30(6): p. 1657-1662.

63. Su, R. J., Overfelt, R. A., and Jemian, W. A. Microstructural and Compositional Transients During Accelerated Directional Solidification of Al-4.5 Wt Pct Cu. Metallurgical and Materials Transactions A-Physical Metallurgy and Materials Science. 1998; 29(9): p. 2375-2381.

64. Hecht, U. and Rex, S. On the Transition from Pushing to Engulfment During Directional Solidification of the Particle-Reinforced Aluminum-Based Metal- Matrix Composite 2014+10 Vol Pct Al2O3. Metallurgical and Materials Transactions A-Physical Metallurgy and Materials Science. 1997; 28(3A): p. 867-874.

65. Lacaze, J. and Lesoult, G. R. J. Experimental Investigation of the Development of Microsegregation During Solidification of an Al-Cu-Mg-Si Aluminum-Alloy. Materials Science and Engineering a-Structural Materials Properties Microstructure and Processing. 1993; 173(1-2): p. 119-122.

66. Ruggiero, M. A. and Rutter, J. W. Microstructure of Bi-Cd-Sn Ternary Eutectic. Materials Science and Technology. 1992; 8(6): p. 523-529.

67. Ruggiero, M. A. and Rutter, J. W. Origin of Microstructure in 350 K Eutectic of Bi-In-Sn Ternary- System. Materials Science and Technology. 1995; 11(2): p. 136-142.

68. Smith, C. S. Some Elementary Principles of Polycrystalline Microstructure. Metallurgical Reviews. 1964; 9: p. 1-48.

69. A. Juarez-Hernandez, H. J. Growth Temperatures and Microstructure Selection During Bridgman Solidification of Hypereutectic Al-La and Al-Ce Alloys. Journal of Crystal Growth. 2000; 208(1): p. 442-448.

70. Hawksworth, A., Rainforth, W. M., and Jones, H. Thermal Stability of Al/Al11Ce3 and Al/Al11La3/Al3Ni Eutectics Obtained by Bridgman Growth. Materials Science and Technology. 1999; 15(6): p. 616-620.

71. Nakagawa, Y. G. and Weatherly, G. C. The Thermal Stability of the Rod Al3Ni-Al Eutectic. Acta Metallurgica. 1972; 20: p. 345-350.

72. Bayles, B. J., Ford, J. A., and Salkind, M. J. The Effects of Elevated-Temperature Exposure on the Microstructure and Tensile Strength of Al3Ni Wisker-Reinforced Aluminum. Transactions of the Metallurgical Society of AIME. 1967; 239: p. 844-849.

73. Smartt, H. B., Tu, L. K., and Courtney, T. H. Elevated Temperature Stability of the Al-Al3ni Eutectic Composite. Metallurgical Transaction. 1971; 2(September): p. 2717-2727.

74. Scheil, E. and Masuda, Y. Rapid Solidification of Al-Fe. Aluminum. 1955; 31: p. 51.

75. Allen, D. R., Gremaud, M., and Perepezko, J. H. Nucleation-Controlled Microstructural Development in Al-Si Alloys. Materials Science and Engineering a-Structural Materials Properties Microstructure and Processing. 1997; 226: p. 173-177.

76. Armstron, G. and Hellawel, A. Composition and Volume Fraction Changes in Ag-Al Eutectic Alloys. Acta Metallurgica. 1974; 22(11): p. 1383-1389.

77. Schnake, F. W. and Varschavsky, G. A. Microstructures of Unidirectionally Solidified Al-Rich Cu-Si Alloys (Reprinted from Metallography, Vol 11, Pg 459-473, 1978). Materials Characterization. 1997; 39(2-5): p. 345-359.

78. Trivedi, R. and Kurz, W. Microstructure Selection in Eutectic Alloy Systems. Solidification Processing of Eutectic Alloys. 1988: p. 3-34.

79. Boettinger, W. J. Growth Kinetic Limitations During Rapid Solidification. *In*: Rapidly Solidified Amorphous and Crystalline Alloys. Kear, B. H., Giessen, B. C., and Cohen, M., Editors. Elsevier: New York, 1981. p. 15-32.

80. Liang, D., Korgul, P., and Jones, H. Composition and Solidification Microstructure Selection in the Interdendritic Matrix between Primary Al3fe Dendrites in Hypereutectic Al-Fe Alloys. Acta Materialia. 1996; 44(7): p. 2999-3004.

81. Pierantoni, M., Gremaud, M., Magnin, P., Stoll, D., and Kurz, W. The Coupled Zone of Rapidly Solidified Al-Si Alloys in Laser Treatment. Acta Metallurgica Et Materialia. 1992; 40(7): p. 1637-1644.

82. Hughes, I. R. and Jones, H. Coupled Eutectic Growth in Al-Fe Alloys .1. Effects of High Growth Velocity. Journal of Materials Science. 1976; 11(10): p. 1781-1793.

83. Jones, H. Observations on a Structural Transition in Aluminium Alloys Hardened by Rapid Solidification. Materials Science and Engineering. 1969; 5(1): p. 1-34.

84. Major, J. F. and Rutter, J. W. Phase Morphology of Pb-Sn-Cd Ternary Eutectic. Materials Science and Technology. 1986; 2(6): p. 534-538.

85. Perez, R., Juarezislas, J. A., and Martinez, L. Quasi-Crystalline Phases in Alloys of Al-Cu-Co-Fe Obtained with a Gravity Chill-Casting Technique. Materials Science and Engineering a-Structural Materials Properties Microstructure and Processing. 1994; 182: p. 837-840.

86. Das, D. K., Prasad, K. S., and Paradkar, A. G. Evolution of Microstructure in Laser-Surface Alloying of Aluminum with Nickel. Materials Science and

Engineering A-Structural Materials Properties Microstructure and Processing. 1994; 174(1): p. 75-84.

87. Gigliott, M. F., Colligan, G. A., and Powell, G. L. F. Halo Formation in Eutectic Alloy Systems. Metallurgical Transactions. 1970; 1(4): p. 891-897.

88. Barclay, R. S., Niessen, P., and Kerr, H. W. Halo Formation During Unidirectional Solidification of Off-Eutectic Binary Alloys. Journal of Crystal Growth. 1973; 20: p. 175-182.

89. Suk, M. J., Choi, G. H., and Moon, I. H. Formation of Halo in Sb-Insb and Sn-Bi Eutectic Alloy Systems. Journal of Crystal Growth. 1992; 123(1-2): p. 5-16.

90. Yilmaz, F. and Elliott, R. Halo Formation in Al-Si Alloys. Metal Science. 1984; 18(7): p. 362-366.

91. Santos, R. J., Kiminami, C. S., and Bolfarini, C. The Liquid Dynamic Compaction of a Zn-Al-Cu Alloy. Materials Science Forum. 1999; 299-300: p. 398-406.

92. Krautwasser, P., Czyrskafilemonowicz, A., Widera, M., and Carsughi, F. Thermal-Stability of Dispersoids in Ferritic Oxide Dispersion-Strengthened Alloys. Materials Science and Engineering a-Structural Materials Properties Microstructure and Processing. 1994; 177(1-2): p. 199-208.

93. Crossman, F. W. and Yue, A. S. Unidirectionally Solidified Ti-Tib and Ti-Ti5Si3 Eutectic Composites. Metallurgical Transactions. 1971; 2: p. 1545-1555.

94. Kraft, R. W., Albright, D. L., and Ford, J. A. Anomalous Thermal Stability of Al-Al2Cu Eutectic Specimens. Transactions of the Metallurgical Society of AIME. 1963; 227: p. 540-542.

95. Stoloff, N. S. Properties and Selection: Nonferrous Alloys and Special-Purpose Materials. *In*: Metals Handbook. Lampman, S. R. and Zorc, T. B., Editors. ASM International: Metals Park, Ohio, 1990. p. 950-980.

96. Oriani, R. Ostwald Ripening of Precipitates in Solid Matrices. Acta Metallurgica. 1964; 12: p. 1399-1409.

97. Speich, G. and Oriani, R. Rate of Coarsening of Copper Precipitates in Alpha-Iron Matrix. Transactions of the Metallurgical Society of AIME. 1965; 233: p. 623-631.

98. Porter, D. A. and Eaterling, K. E. Phase Transformations in Metals and Alloys. Chapman & Hall: New York, 1992.

99. Kraft, R. W. AND Albright, D. L. Microstructure of Unidirectionally Solidified, Al-CuAl2 Eutectic. Transactions of the Metallurgical Society of AIME.1961; 221: p. 95-102.

100. Tewari, S. N. Directionally Solidified Iron-Base Eutectic Alloys. 1976, National Aeronautics and Space Administration: Springfield. vol. NAS 1.14:D-8354.

101. Tewari, S. N. Directionally Solidified Eutectic Alloy [Gamma-Beta]. 1977, National Aeronautics and Space Administration: Springfield. vol. NAS 1.14:D-8355.

102. Stone, I. C. and Jones, H. Effect of Cooling Rate and Front Velocity on Solidification Microstructure Selection in Al-3.5wt%Fe-O to 8.5wt%Si Alloys. Materials Science and Engineering A-Structural Materials Properties Microstructure and Processing. 1997; 226: p. 33-37.

103. Gutmanas, E. Y., Botstein, O., and Lawley, A. Elevated Temperature Stability of Powder Processed Al-Fe-Ni. International Journal of Powder Metallurgy. 2000; 36(2): p. 47-55.

104. Davies, I. G. and Hellawel.A. Structure of Directionally Frozen Al-Cual2 Eutectic Alloy. Philosophical Magazine. 1969; 19(162): p. 1285-1297.

105. Harf, F. H. A Directionally Solidified Iron-Chromium-Aluminum-Tantalum Carbide Eutectic Alloy. 1977, National Aeronautics and Space Administration: Springfield. vol. NAS 1.15:X-3434.

BIOGRAPHICAL SKETCH

Eric John Fodran, originally from California, obtained his undergraduate degree in materials science in 1994 from California Polytechnic University at San Luis Obispo, and later received his M.S. degree in materials science in 1997 from the same university.

He entered the graduate program in the Department of Materials Science and Engineering, at the University of Florida in 1997, with interests in the pursuit of research in the field of metallurgy. Specifically, his interests are focused in processing, microstructural evolution and rapid solidification. Under the guidance of Dr. M. J. Kaufman he has obtained a Ph.D. degree in the Department of Materials Science and Engineering.

I certify that I have read this study and that in my opinion it conforms to acceptable standards of scholarly presentation and is fully adequate, in scope and quality, as a thesis for the degree of Doctor of Philosophy.

Michael J Kaufman, Chairman
Professor of Materials Science and Engineering

I certify that I have read this study and that in my opinion it conforms to acceptable standards of scholarly presentation and is fully adequate, in scope and quality, as a thesis for the degree of Doctor of Philosophy.

Reza Abbaschian
Professor of Materials Science and Engineering

I certify that I have read this study and that in my opinion it conforms to acceptable standards of scholarly presentation and is fully adequate, in scope and quality, as a thesis for the degree of Doctor of Philosophy.

Gerhard E. Fuchs
Assistant Professor of Materials Science and Engineering

I certify that I have read this study and that in my opinion it conforms to acceptable standards of scholarly presentation and is fully adequate, in scope and quality, as a thesis for the degree of Doctor of Philosophy.

Paul H. Holloway
Professor of Materials Science and Engineering

I certify that I have read this study and that in my opinion it conforms to acceptable standards of scholarly presentation and is fully adequate, in scope and quality, as a thesis for the degree of Doctor of Philosophy.

Timothy J. Anderson
Professor of Chemical Engineering

This dissertation was submitted to the Graduate Faculty of the College of Engineering and to the Graduate School and was accepted as partial fulfillment of the requirements for the degree of Doctor of Philosophy.

August 2002

Pramod P. Khargonekar
Dean, College of Engineering

Winfred M. Phillips
Dean, Graduate School